UCLA
UCLA Electronic Theses and Dissertations

Title
Integration of Sensory and Temporal Information in CA3

Permalink
https://escholarship.org/uc/item/06x7c4pj

Author
Cheung, Stephanie Karyun

Publication Date
2022

Peer reviewed|Thesis/dissertation

eScholarship.org Powered by the California Digital Library
University of California

UNIVERSITY OF CALIFORNIA

Los Angeles

The integration of sensory and temporal information in CA3

A dissertation submitted in partial satisfaction of the

requirements for the degree

Doctor of Philosophy in Neuroscience

by

Stephanie Karyun Cheung

2022

© Copyright by

Stephanie Karyun Cheung

2022

ABSTRACT OF THE DISSERTATION

Integration of Sensory and Temporal Information in CA3

by

Stephanie Karyun Cheung

Doctor of Philosophy in Neuroscience

University of California, Los Angeles, 2022

Professor Peyman Golshani, Chair

Memories are temporally organized. When recalling an event, we also recall the relative timing it was experienced. How does the brain compute and store this temporal representation of memory? The hippocampus is important to the temporal organization of memories. Hippocampal CA1 or CA3 lesions cause impaired coding of sequential events separated by time. The hippocampus bridges stimuli-free gaps between sequential events through neural ensembles that fire sequentially during the delay. These “time cells” fire sequentially encoding successive moments during the delay. Recent work has found that the CA1 region of the hippocampus contains neurons that display stimulus-specific sequential firing patterns during the delay period of a working memory task. CA1 largely lacks recurrent connectivity, so it is unlikely that it generates these sequential firing patterns on its own. CA3 is an upstream region with direct connections through the Schaffer collaterals to CA1. CA3 has extensive recurrent connections and is a likely candidate that generates these stimulus-specific sequential firing patterns. The recurrent connections in CA3 are well-suited for storing and processing temporal information because they allow for rapid associations. CA3 also receives input from the lateral entorhinal cortex, which processes nonspatial sensory information and receives direct connects from the olfactory bulb. To date, it is

unknown where and how sensory and temporal information is integrated. Given the unique attributes of CA3, we propose that CA3 is where sensory and temporal information is integrated and that this code is then passed onto CA1. To test this hypothesis, we used cutting-edge chronic *in vivo* two-photon calcium imaging to monitor CA3 neuronal populations during a working memory task. We demonstrate that CA3 contains populations of cells that hold time and odor information. These cells fired in a stimuli-specific sequential manner during a working memory task. Though these odor-specific sequence cells were found to have low odor selectivity, we were able to decode odor and time from their firing activity. The odor-specific time cells in CA3 did not increase in numbers across days. These experiments help shed light on how elements of a memory are unified and coded within CA3.

The dissertation of Stephanie Karyun Cheung is approved.

Alcino Jose Silva

Laura Anne Wilke

Dean Buonomano

Anne Kathryn Churchland

Peyman Golshani, Committee Chair

University of California, Los Angeles

2022

DEDICATION

I dedicate this dissertation to my grandma. She passed before she could see me complete my degrees. She was always so proud of me and the things I accomplished. I wear a college class ring every day. People probably look at it and think, “Wow, she really liked her college.” This is not the reason I wear it. I have this ring because when I graduated from college my grandma was so proud because my siblings and I were the first in our family to do so. She offered to buy me a class ring or gift me the monetary equivalent of it. I chose the ring because I wanted something solid that would remind me of her. The more I wore it, the more it became like an armor to me. When I am at work or about to enter a difficult situation and feel unsure or insecure, I touch it. I then I am reminded of how proud my grandma is of me, of how she believed in me, and that I come from her line--a line of women who come out on top of hard situations with grace and resilience. Then, I feel her with me, and nothing can touch me. In being proud of me, she taught me to be proud of myself. She showed me unconditional love and modeled what a strong woman looked like. I will keep her memories in my mind, her love close to my heart, and her pride on my finger, always.

TABLE OF CONTENTS

LIST OF FIGURES

LIST OF ABBREVIATIONS

2P: two-photon

CA1: cornu Ammonis 1

CA2: cornu Ammonis 2

Ca^{2+}: calcium ions

CA3: cornu Ammonis 3

DAPI: 4′,6-diamidino-2-phenylindole

DG: dente gyrus

DNMS: delayed-non-match-to-sample

GECI: genetically encoded calcium indicator

GFP: green fluorescent protein

LEC: lateral entorhinal cortex

PBS: phosphate buffered saline

PFA: paraformaldehyde

ROI: region of interest

SD: standard Deviation

SI: selectivity index

SVM: support vector machine

ACKNOWLEDGEMENTS

When I began my graduate school journey, I prepared myself for the difficulties I would encounter: the failed experiments, the long hours, the rigorousness of science, having to create something from nothing. Looking back, those were the easiest parts of my PhD. Being a woman in STEM is at once an extremely isolating, yet bonding experience. I have had the opportunity to take part in and, even, grow a community of women scientist. Yet, graduate school was also when I felt the loneliest (and that was not just because I spent months working the graveyard shift in a dark 2P room with only mice to keep me company). I was naïve. As many of us in science did, as a child, I dreamt of being a 'mad scientist' running countless interesting and diabolical experiments. I did not conceive that a lab meant more than just a collective of individuals running independent projects. It was only in graduate school that I understood: no person is an island. Or at least, no person is an efficient, productive, happy island. Your community matters. Your environment matters. If I have learned anything in these four years, I have learned that you do not have to do everything yourself. Find your allies, find your community. Their strength is yours too, and together the sum is greater than the parts. This has been a hard year. While this PhD is an important and big thing that I have done, it is small in comparison to real life itself. In academia, we often have a myopic view that our field, our lab, and our experiments are our whole world when, in reality, they are a miniscule part a larger world. The bigger part of life exists outside of lab. It is this bigger part that has helped me through the hardest parts of this PhD by reminding me that these experiences do not define me. I am more than what I produce. How I have been treated is not indicative of what I deserve. The most

valuable skills I have gained during this time have nothing to do with science as most would define it, but are the very ones that will make me a better scientist.

That is not to say I have not encountered some wonderful humans along the way. Let me spend the pages I have to give my thanks to them. I thank my friends and colleagues in the lab that have offered me their advice and companionship. Thank you to Pingping Zhao, Hesper Chen, and Celina Yang for all the lunches and laughter we shared. When I first rotated in the lab in 2017, I worked with Pingping, and she always has been one of the most hardworking, rigorous scientists. I will miss our snack exchanges and all the times you cooked delicious food for me. That food sustained me through long, cold lab hours. Conor Dorian, thank you for joining the lab so that we could not only be in the same PhD class, but also in the same lab. Thank you for always being willing to talk through my wild project hypotheses and suffering through my venting about coding and equipment troubleshooting. Thank you for taking care of our succulent that I forced you to co-adopt, and which I subsequently abandoned. Thanks to my future co-first author and my collaborator Mina Shahi for giving me hope for collaborations. Thank you for validating my amateur coding. Thank you for staying up all those nights with me, going slightly mad as we poured over analysis. You are one of the best coders I know, and I am honored to be able to work with you. I look forward to what we will create together. Thank you to the bright undergraduates that I had the pleasure of working with: Muskaan Mehra, Jonathan Kermanshahchi, and Farhaz Shaikh. Thank you to Karen Safaryan, Arash Bellafard, and Ronen Reshef for their advice on analysis.

Chapter 2 and 3 of this dissertation will form part of a paper entitled, “Integration of Sensory and Temporal Information in CA3,” on which I will be first author. I performed all surgeries, imaging, behavioral assays and collected all the data described. I also developed a calcium imaging analysis pipeline detailed in these chapters, which was later validated. My co-first author will be Mina Shahi, who has helped immensely with analysis and coding.

My thesis work was supported by the David Geffen Medical Scholarship, a NIH National Institute of Mental Health (NIMH) Ruth L. Kirschstein Individual Predoctoral NRSA for MD/PhD Fellowship (NIH F30MH125638), as well as the UCLA Medical Scientist Training Program (MSTP) (T32-GM008042). I am grateful for the opportunities I have been allowed to pursue through these funding sources.

As a UCLA-Caltech MSTP student, I have had the unique position of being a part of many different communities. I thank the leadership and administration of UCLA MSTP: Dr. Carlos Portera-Cailliau, Dr. Karen Reue, Dr. Olujimi Ajijola, Susie Esquivel, and Staci Chikami. Thank you to Dr. Maureen Su, UCLA-Caltech MSTP associate director, who comforted me during difficult parts of my graduate studies and for always supporting women. Thank you to my thesis committee for their guidance. I thank Dr. Alcino Silva for his warmth and for his unwavering belief in me from the very beginning. Some of my fondest memories are from my 2018 rotation in the Silva lab. Thank you to the UCLA Interdepartmental Ph.D.

Program for Neuroscience (NSIDP) and my NSIDP classmates. I thank Dr. Felix Schweizer, chair of NSIDP, for being an open ear and for his efforts in mediation. Thank you for always making time to meet with me, for being willing to pursue unorthodox solutions, and for always checking up on me. I thank Jenny Lee, NSIDP graduate advisor, who has helped me to navigate much of graduate school. I thank Dr. Greg Payne for supporting students and trying to create an avenue to combat mistreatment. I have always appreciated your humor, positivity, and willingness to take up a difficult task. I thank Mohammad Cato, Title IX Director at UCLA. I thank Dr. Dave MacIntosh, Vice Dean for Justice, Equity, Diversity, and Inclusion at the David Geffen School of Medicine (DGSOM) at UCLA. I thank Jenny Lee, academic case manager at UCLA. I thank Dr. Samantha Butler for being my advocate. Often, those in higher positions shut the door instead of opening it for those below them. Samantha is not one of those people. I hope we can work together in better circumstances in the future.

I want to especially thank Dr. Iljie Fitzgerald, Assistant Dean for Student Affairs at DGSOM, for looking after me all these years. I met Iljie during my preclinical medical school years. I thought that I would not see her after I left to pursue my PhD, but Iljie has been by my side through all my struggles, going above and beyond what has been asked of her. Thank you for showing me that kindness and strength can go hand-in-hand. Thank you for always being in my corner. Thank you for always being ready to fight for me even when I was not ready to fight for myself. I aspire to be the type of mentor that you are to me.

I thank my friends who have tolerated me through my graduate years and beyond. Thank you to Kevin Tang, Michael Hui, Kevin Do, Jasmine Chen, Triet Do, Kristine Huynh, and Sarah Moore. Kevin and Mike, I am so glad we found each other in medical school, even though my mom still can't tell you guys apart. Our friendship can't be discarded like a Salt n Straw $5 ice cream cone thrown out the window of a moving vehicle. May the best of our todays be the worst of our tomorrows.

Kaleab Tessema and David Shia, thank you for all the late-night taco runs. Kaleab, thank you for always showing me that it is possible to do things differently, but still do it well. When I see you succeed, I believe that I can as well. Thank you for your constant emotional strength, your night-owl tendencies that match mine, and for just always being the best person. Bryce Bajar, thank you for your keen scientific advice. You are the person that every MSTP or PhD program wishes they could duplicate about a hundred times over.

Eta Atolia and Isaura Frost, thank you for being in my MSTP class. There are no other people I would choose to walk this journey with. That being said, I forgive you both for leaving me behind. Eta, thank you for choosing to join this program, for being roommates with me, for joining a lab in the same building as mine. I still can't believe how well we clicked from the first night we met. There is no one I trust more. Thank you for teaching me what love is. Or I'm guessing that is what you were trying to do after forcing me to watch 200+ romcoms. I can't wait to embarrassingly cheer at your upcoming thesis defense.

Simone Chung and Steve Chung, thank you for opening your hearts and your home to me. I can't fully express my appreciation to you both in these words enough. Thank you for always pushing me beyond my comfort zone. Thank you for giving me a community and family. Thank you for taking me in during my lowest moments. Thank you for showing me a different way to see the world. Simone, thank you for our 10+ year long friendship. The person I was when we met is not the same one that is finishing this PhD. I hope you will continue to watch as I grow as a person. Thank you to Natasha Yamane. I truly believe every person should have friends they can share anything with—from what you ate this morning to the last thing that made you cry. Simone and you are this to me. Gabriel Fernandez and David James thank you for working out with me, which kept me sane. Seadimo Tlale thank you for your words.

I thank my parents, Elena Chan and Nelson Cheung, who have given up so much just so I could have a chance to succeed. Thank you for always trying your best to support me. Thank you for making a home in a foreign land. Thank you to my mom who has always been just one phone call away. Thank you to my brothers, Christopher Cheung and Alexander Cheung, for their support. Thank you to my younger brother, Alex, who has always been the best of us siblings. Thank you for being always kind, considerate, and the person who can make me laugh in any situation. Thank you for bringing Miji Kim into our family. Thank you to my uncles, Lewis Chan and Kai Chan. Thank you to the rest of my family in San Francisco, who have watched over me from when I was a child to this day.

I have heard it said that it takes a village to raise a child. It is also said that the child who is not embraced by the village will burn it down to feel its warmth. I am thankful for the village that I have built. I urge you to create a world around you which reflects your vision for the future. If your village does not accept you, burn it down. Make one that will. You do not have to accept the space you are given. Often, you will feel that you do not belong. Remember, spaces were often not created with minorities and women in mind. Acknowledge this truth rather than internalizing it. Surround yourself with people who truly see and understand you. The goal should always be to be able to be your most free and true self. For this, I am thankful to my family, both born into and built. I am thankful for my work with the UCLA Womxn in MSTP committee. I was there at the creation of this committee and have had the privilege to watch it grow into a vibrant community of women and a safe space for us to gather. As chair, at every event we held, I had women come up to me to share stories that were sadly too common and familiar. The work I have done with this committee is among that which I am most proud. I thank every woman and ally that was a part of this experience.

VITA

EDUCATION

2010 – 2011	University of California, Berkeley
2011 – 2013	Columbia College, Columbia University ▪ B.A. in Neuroscience and Behavior
2014 – 2015	School of Continuing Education, Columbia University
2016 –	David Geffen School of Medicine, University of California, Los Angeles Medical Scientist Training Program, Interdepartmental Program in Neuroscience

RESEARCH EXPERIENCE

2010	Summer Undergraduate Research Fellowship (Yonas Geda, M.D., advisor) Alzheimer's Disease Research Center, Mayo Clinic
2011	Gazzaley Lab (Judy Pa, M.D., advisor) University of California, San Francisco Medical Center
2010 – 2012	Subarachnoid Hemorrhage Outcomes Project (Hector Lantigua, M.D., advisor) New York Presbyterian Hospital, Columbia University Medical Center
2011	Mucke Lab (Dena Dubal, M.D.-Ph.D., advisor) Gladstone Institute of Neurological Disease, University of California, San Francisco Medical Center
2012 – 2015	Siegelbaum Lab (Steven Siegelbaum, Ph.D., advisor) Columbia University Medical Center
2015-2016	Basu Lab (Jayeeta Basu, Ph.D., advisor) New York University Langone Medical Center
2018	Silva Lab (Alcino Silva, PhD., advisor) Department of Neurobiology, UCLA

2018-2022 Golshani Lab (Peyman Golshani, M.D.-Ph.D., advisor)
Department of Neurology, UCLA David Geffen School of Medicine

PUBLICATIONS

1. Basu, J., Zaremba J.D.*, **Cheung, S.K.***, Hitti F.L, Zemelman B.V., Lonsonzy A., Siegelbaum S.A. (2015) Tuning Hippocampal Activity, Sensory Coding and Learning Behavior with Entorhinal Cortex Long-Range Inhibition. Science. *These authors contributed equally.
2. Rosen, Z.B., **Cheung, S.K.**, and Siegelbaum, S.A. (2015) Dopaminergic inputs regulate excitation of CA1 neurons. Nature Neuroscience.
3. Kupferman J., Basu J., Russo M.J., Guevarra J., **Cheung, S.K.**, Siegelbaum S.A. (2014) Reelin Signaling is Required for the Enrichment of Ion Channels in Pyramidal Neuron Distal Tuft Dendrites. Cell.
4. Basu, J., Srinivas K. V., **Cheung, S.K.**, Taniguchi, H., Huang, Z. J., and Siegelbaum S.A. (2013) A cortico-hippocampal learning rule enhances information flow through the hippocampal circuit by shaping local inhibitory microcircuit activity. Neuron. Cover Illustration.

PRESENTATIONS

Selected oral presentations

1. **Cheung SK**. Integration of Sensory and Temporal Information. UCLA-Caltech Medical Scientist Training Program Tutorial Series, October 12, 2020.

Selected poster presentations

1. **Cheung SK**. Integration of Sensory and Temporal Information. Society for Neuroscience, Annual Conference, November 10, 2021.
2. **Cheung SK**. Integration of Sensory and Temporal Information. UCLA Brain Research Institute 32nd Annual Neuroscience Poster Day, November 30, 2021.

SELECTED HONORS AND AWARDS

2016 David Geffen UCLA MSTP Scholar

2020 NIH National Institute of Mental Health (NIMH) Ruth L. Kirschstein Individual Predoctoral NRSA for MD/PhD Fellowship (NIH F30MH125638)

2021 UCLA Brain Research Institute and Semel Institute for Neuroscience & Human Behavior Student Travel Award for the Annual Society for Neuroscience Meeting

Chapter 1

Introduction

“All memory, therefore, implies a time elapsed; consequently only those animals which perceive time remember, and the organ whereby they perceive time is also that where by they remember”

- Aristotle, On Memory and Reminiscence

1.1 HIPPOCAMPUS AND TIME

Memories are experienced and encoded along the axis of time (Tulving, 1984). We remember not only what experiences we have had in the past, but the sequential order and relative timing in which they were experienced. How and where temporal information is represented and paired with corresponding external stimuli is still incompletely understood.

The first step to answering this question is identifying the brain region essential to memory formation. This question was famously addressed in the 1950s with patient H.M. Patient H.M., who suffered from severe epileptic seizures and underwent bilateral hippocampi lesions. This experimental treatment left him with anterograde amnesia, unable to form new memories (Scoville and Milner, 1957). Thus, the hippocampus became known as a region important to memory. Only recently has it been understood that the hippocampus also processes temporal information.

The hippocampus has been proposed to carry information on the positions of elements in sequences (Eichenbaum, 2013). A study on a patient with selective bilateral hippocampal lesions found disruptions in temporal order memory. The patient performed worse compared to controls when identifying the correct order of word-pairs in a list (Mayes et al., 2001). Lesions in the hippocampal subregions CA1 and CA3 impair memory of the sequential order of events (Fortin et al., 2002; Farovik et al., 2014). Imaging studies of the hippocampus using fMRI found that hippocampal activity patterns reflected the temporal

position of objects in a sequence (Hsieh et al., 2014). These studies along with others gave rise to the theory that the hippocampus plays a critical role in the organization of memories in time (Eichenbaum, 2014; Eichenbaum, 2013; Kraus et al., 2013).

How does the hippocampus represent these temporally organized sequential events? Early studies in the prefrontal cortex of monkeys showed persistent firing in the period between events (Fuster and Alexander, 1971). It was thought that this persistent activity was how information was maintained without an external cue (Constantinidis et al., 2018). Later theories postulated that information was maintained through a temporally dynamic code rather than a stable persistently firing population (Sreenivasan et al., 2014). This reasoning carried over to how the neural representations of sequential events were thought of in the hippocampus. The hippocampal neural representation of sequential memories is thought to occur through either (1) a neuronal ensemble that creates a temporally organized firing chain, in which each neuron represents a temporally distinct event or (2) a neuronal ensemble that gradually evolves to fit the temporal context (Eichenbaum, 2013). It is still unknown precisely how these representations emerge and are maintained in the hippocampus.

1.2 SEQUENTIAL FIRING PATTERNS IN THE HIPPOCAMPUS

Further studies have shown that the hippocampus bridges temporal gaps between serial stimuli in the absence of external cues through neural ensembles that fire sequentially during the delay period (Eichenbaum, 2013; Itskov et al., 2011; Naya et al., 2011; MacDonald et al., 2011; Modi et al., 2014). These "time cells" encode successive moments during the delay period (Lundqvist et al., 2018; Pastalkova et al., 2008; MacDonald et al., 2011). Yet, the mechanisms that create these temporal representations, and the role of the specific Hippocampal subfields in establishing and remapping these stimulus-specific time fields is still not known.

Within the subregions of the hippocampus, stimulus-specific sequential firing patterns have been found in hippocampal CA1 during the delay period of working memory tasks (**Fig. 1.1**) (Pastalkova et al., 2008; MacDonald et al., 2011). These sequentially firing cells can be split into two subsets of cells that emerge from the pyramidal neurons: stimuli-specific cells and stimuli-specific time cells. The stimuli-specific cells are active during the presentation of an external stimuli, encoding stimuli-related cues such as odor or object identity (MacDonald et al., 2011). These stimuli-specific cells were reliably activated across nearly all trials of the task and their numbers remained stable through learning and across days (Taxidis et al., 2020). Stimuli-specific time cells were active during the delay period and encoded stimuli-specific time points. Each unique stimuli triggered a specific sequence of time cell firing that tiled the delay (**Fig. 1.1**). Stimuli-specific time cells were found to be unstable across trials and increased in number during learning and across days (Taxidis et al., 2020).

While the hippocampus is known to be a sequence generator (Pastalkova et al., 2008), it is unclear how these stimulus-specific firing patterns emerge in CA1. CA1 is mainly connected through feedforward connections that lack the recurrent connectivity that would allow for sequence generation. The unstable odor-specific time cells also do not hold a stable code that can reliably pass temporal information. Where are stable, stimulus-specific sequences which hold temporal information generated and integrated with sensory information?

Figure 1.1.

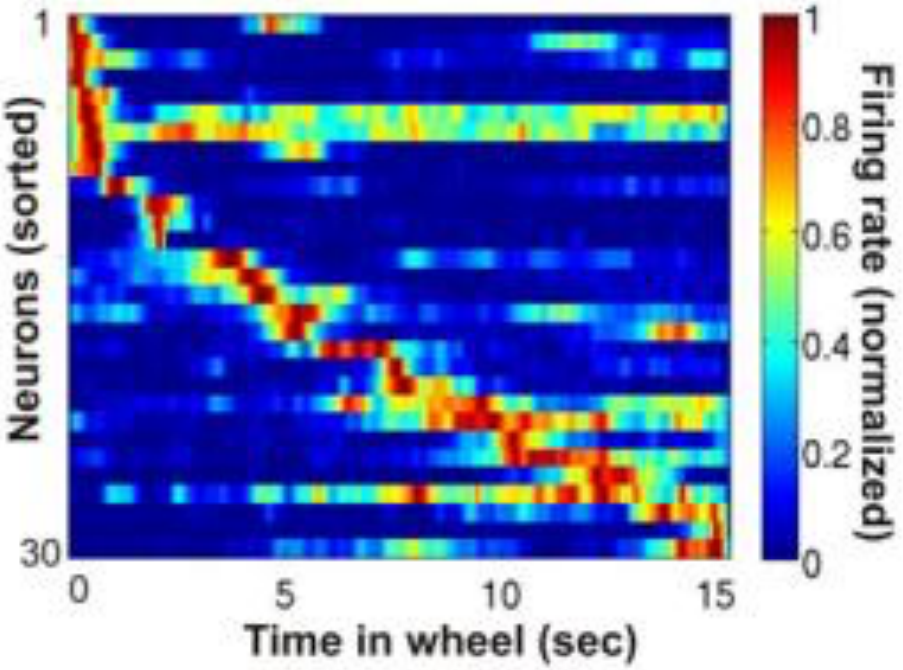

Figure 1.1. Hippocampal neurons fire sequentially across the delay. Normalized firing rate of 30 simultaneously recorded neurons during wheel running, ordered by peak firing rate latency. Each row represents the activity of one neuron. Figure adapted from Pastalkova et al. 2008.

1.3 CA3 CONNECTIVITY

The hippocampus is split into five main subregions: subiculum, CA1, CA2, CA3, and the dentate gyrus (DG). CA1 is considered the main output of the hippocampus. As such, CA1 receives many inputs from within and outside of the hippocampus. Two important inputs to CA1 originate from the entorhinal cortex. The first input, the monosynaptic pathway, comes directly from entorhinal cortex layer III to CA1. The second input is called the trisynaptic loop. The trisynaptic loop begins in entorhinal cortex layer II and travels to DG through the perforant path (Fig. 1.2). From the dentate gyrus, it projects to CA3 through the mossy fibers. Finally, CA3 sends axons through the Schaffer collaterals to CA1 pyramidal neurons (Deng et al., 2010).

CA3 is positioned directly upstream of CA1 in the trisynaptic pathway and likely relays important information to CA1. Compared to all other major extrinsic inputs to CA1, CA3 sends the strongest excitatory connections to CA1 via the Schaffer collaterals and commissural input (Sun et al., 2014). A single CA1 pyramidal neuron receives input from approximately 5,500 CA3 cells (Amaral et al., 1990). Intact CA3 to CA1 connection in the trisynaptic pathway is necessary for rapid one-trial learning, pattern completion-based memory recall, and spatial tuning of CA1 cells (Nakashiba et al., 2008; Nakashiba et al. 2009).

The CA3 to CA1 pathway could carry stimuli-specific time-delay information such as odor. The lateral entorhinal cortex (LEC) receives direct input from the olfactory bulb and has been

implicated in odor-specific olfactory coding (Xu et al., 2012; Leitner et al., 2016). Since this indirect pathway originates in the LEC, it contains odor-specific information and passes through CA3. Odor-specific information can be further encoded with time delay information in CA3. CA3 could then pass the integrated information to CA1 through the Schaffer collaterals. In fact, inhibiting CA3 has been found to abolish temporal coding in CA1 (Middleton et al., 2016).

There are approximately 303,930 CA3 pyramidal cells (Amaral et al., 1990). CA3 pyramidal cells receive two distinct excitatory inputs. One input is the mossy fibers from the DG. These mossy fibers contact CA3 apical dendrites close to the soma. Activation of these fibers can trigger fast, strong responses in the CA3 soma. The second input comes from recurrent connections. CA3 has a unique architecture of extensive recurrent connections: 30-70% of synapses on CA3 dendrites originate internally from other CA3 cells (Li et al, 1994). These recurrent connections contact the CA3 dendrites more distally compared to the mossy fibers. It has been suggested that this results in weaker, slower responses in the CA3 soma (Le Duigou et al., 2014). Though they may be weaker, recurrent connections contact many more CA3 dendrites than mossy fibers. A single DG granule cell makes 10-20 synapses on approximately 14 CA3 pyramidal cells through mossy fibers (Clairbourne et al., 1986; Amaral et al., 1990). Each CA3 cell is innervated by approximately 46 DG granule cells (Amaral et al., 1990). Recurrent connections can make several thousand synapses on a much larger population of CA3 pyramidal cells; a single CA3 pyramidal cells is innervated by approximately 6000 other CA3 pyramidal cells (Amaral et al., 1990). This is 1.9% of the

whole CA3 pyramidal cell population (Amaral et al., 1990). One DG cell can cause a CA3 pyramidal cell to fire through one mossy fiber input (Henze et al., 2002). Multiple active recurrent synapse inputs are required to cause a CA3 pyramidal cell to fire (Miles and Wong, 1987).

CA3 has access to sensory information from the LEC through the trisynaptic pathway. Through its recurrent connections it has the means to generate an internal temporal signal. CA3 could potentially generate a stable sequence integrating sensory and temporal information and pass this sequence onto CA1 through the trisynaptic pathway.

Figure 1.2.

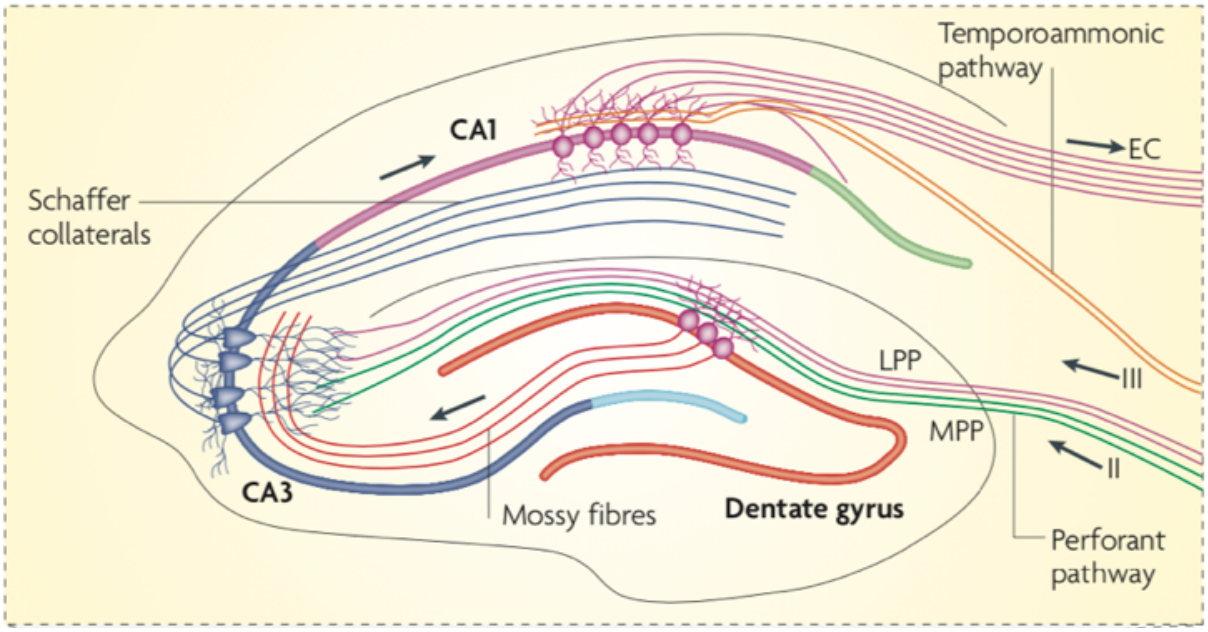

Figure 1.2. Neural Circuitry in the Hippocampus. Figure adapted from Deng et al. 2010.

1.4 CA3 AS AN ATTRACTOR NETWORK

Axons of CA3 pyramidal cells make excitatory synapses with other CA3 pyramidal cells, forming a recurrent network. The recurrent network in CA3 acts as an attractor network (Treves and Rolls, 1992). An attractor network is a neural network that has one or more stable states of neuronal firing patterns (Hopfield, 1982). The stability of these states is determined by the strength of recurrent connections between the neurons in the network. Synaptic links are strengthened between CA3 neurons that represent different components of a memory through Hebbian long-term potentiation dependent on presynaptic and postsynaptic activity (Liseman, 1999). Incoming activity "attracts" the network into one of the stable states (Rolls, 2013). Importantly, activation of a few neurons can reactivate an entire stable state (Liseman, 1999; Guzman et al., 2016; Rebola et al., 2017) consisting of stimulus-specific sequences that help to maintain information. Therefore, the attractor network allows for generation of intrinsic sequences (Pastalkova et al., 2008).

Due to the robust auto-associative network, rapid one-trial associative learning can occur over seconds (Remaud et al., 2014) and this encoding of information can be efficiently done through small CA3 neuronal ensembles (Guzman et al., 2016). Thus, CA3 can generate intrinsic stable sequences through its attractor network within a rapid timeframe. But does CA3 process temporal information?

1.5 TIME CELLS IN CA3

Most studies to date have focused on CA1 and CA2 for temporal processing, but a recent study using implanted electrodes in rats completing a working memory task found cells in CA3 that exhibit robust temporal modulation similar to those found in CA1(Salz et al., 2016). These CA3 time cells displayed a sequential firing pattern during the delay of the working memory task, mirroring CA1 cell activity. More CA3 time cells were active in the early delay. A similar proportion of CA3 time cells were identified compared to CA1 time cells (Salz et al., 2016). These CA3 time cells seem to be more stable than CA1 cells over time (Dong and Sheffield, 2021). Though CA3 seems to process sensory and temporal information, it is not known if CA3 is where integration of these two occurs.

1.6 SUMMARY

Memories are experienced, encoded, and stored in a sequential manner along the axis of time. How and where this temporally dynamic information is represented and paired with external stimuli is still incompletely understood. The hippocampus is critical to temporal organization of memories (Eichenbaum, 2013; Eichenbaum, 2014; Kraus et al., 2013). It bridges gaps between sequential events through neural ensembles that fire sequentially in the delay between stimuli (Eichenbaum, 2014; Itskov et al., 2011; Naya et al., 2011; Modi et al., 2014). These “time cells” can encode both the item remembered and the time elapsed after the stimulus (Lundqvist et al., 2018; Pastalkova et al., 2008; Macdonald et al., 2011). The neurobiological mechanisms that create these temporal representations, the specific hippocampal subfield in which they originate, and the rules governing their remapping and usage are unknown.

The CA1 region of the hippocampus contains neurons that fire selectively to stimuli and other groups of neurons that fire at specific times after the delay duration during a working memory task (Pastalkova et al., 2008; MacDonald et al., 2011). A downstream region, reading out the population activity patterns, can decode both the identity of the stimulus and the elapsed time after the first stimulus was encountered. These sequences arise after training on the task, while sensory responses are present even before training (Taxidis et al., 2020).

Yet, it is still unclear how these stimulus-specific sequences arise in hippocampal CA1. As CA1 largely lacks recurrent connectivity, it is unlikely that it can generate sequential firing on its own. One candidate region that could generate stimulus-specific sequences is CA3. CA3 axon collaterals called the Schaffer collaterals communicate with CA1 pyramidal neurons (Deng et al., 2010). CA3 has a unique architecture of extensive recurrent connections (Treves and Rolls, 1992). These recurrent connections allow for rapid associations, such as between time and an object or reward (Fuster and Alexander, 1971). This system is inherently suited for storing and working with temporary information (Rolls, 2013). These attributes point to CA3 potentially playing an important role in encoding time. CA3 also receives input from the lateral entorhinal cortex, which processes nonspatial sensory information and receives direct connections from the olfactory bulb (Xu and Wilson, 2012; Leitner et al., 2016). The overarching hypothesis of this thesis project is that sensory information and time is integrated as a stable code in CA3 and then passed to CA1.

1.7 RATIONALE FOR THESIS PROJECT

While there have been time cells identified in CA3, the tasks used in these studies are all spatially based. It is not yet known if CA3 holds nonspatial temporal information. This is important because historically, it has been hard to disentangle spatial cues, such as distance, from timing cues. It is possible that the hippocampus acts as a path integrator, regardless of whether the path is along distance or time. Using a nonspatial task helps to better isolate and measure temporal signals. It would also expand the CA3 field of study, which has focused on CA3 as mainly a region for processing spatial information.

The studies done in CA3 have mainly been done through electrode recordings. This method did not allow cells to be followed across days. This study would be the first to use two-photon calcium imaging to image and follow CA3 time cells across days. Dong and Sheffield et al. 2021 also used two-photon calcium imaging, but they used a spatial task and imaged place cells.

This study used a novel method in combining two-photon calcium imaging with an intersectional approach to targeting CA3. I utilized transgenic mice that expressed *Cre* in CA3 combined with a FLEXed virally expressed calcium indicator. This way, the calcium indicator only expressed in CA3. This is important and novel because previous studies injected a non-flexed calcium indicator into the CA3 region. Since CA2 neighbors CA3, unintended infection of CA2 cells was likely. When imaging this mixed population of

CA2/CA3 cells it was impossible to distinguish between the two. Thus, it was hard to make specific claims regarding CA3 based on the previous imaging findings.

This thesis project helps shed light on how the brain processes time and melds it to external stimuli to create a memory tagged within a moment in time.

1.8 REFERENCES

Amaral, D.G., Ishizuka, N. & Claiborne, B. Neurons, numbers and the hippocampal network. *Prog. Brain Res.* 83, 1–11 (1990).

Claiborne B. J., Amaral D. G., Cowan W. M. (1986). A light and electron microscopic analysis of the mossy fibers of the rat dentate gyrus. *J. Comp. Neurol.* 246 435–458 10.1002/cne.902460403

Deng W, Aimone JB, Gage FH. New neurons and new memories: how does adult hippocampal neurogenesis affect learning and memory? Nat Rev Neurosci. 2010 May;11(5):339-50. Doi: 10.1038/nrn2822. Epub 2010 Mar 31. PMID: 20354534; PMCID: PMC2886712.

Eichenbaum H. Memory on time. Trends Cogn Sci. 2013 Feb;17(2):81-8. Doi: 10.1016/j.tics.2012.12.007. Epub 2013 Jan 12. Erratum in: Trends Cogn Sci. 2013 May;17(5):255. PMID: 23318095; PMCID: PMC3558533.

Eichenbaum H. Time cells in the hippocampus: a new dimension for mapping memories. Nat Rev Neurosci. 2014 Nov;15(11):732-44. Doi: 10.1038/nrn3827. Epub 2014 Oct 1. PMID: 25269553; PMCID: PMC4348090.

Farovik A, Dupont LM, Eichenbaum H. Distinct roles for dorsal CA3 and CA1 in memory for sequential nonspatial events. Learn Mem. 2009 Dec 22;17(1):12-17. Doi: 10.1101/lm.1616209. PMID: 20028733; PMCID: PMC2807176.

Fortin NJ, Agster KL, Eichenbaum HB. Critical role of the hippocampus in memory for sequences of events. Nat Neurosci. 2002;5(5):458-462. Doi:10.1038/nn834

Fuster JM, Alexander GE. Neuron activity related to short-term memory. Science. 1971. 173(3997):6524. PubMed PMID: 4998337.

Guzman SJ, Schlögl A, Frotscher M, Jonas P. Synaptic mechanisms of pattern completion in the hippocampal CA3 network. Science. 2016 Sep 9;353(6304):1117-23. Doi: 10.1126/science.aaf1836. PMID: 27609885.

Henze, D., Wittner, L. & Buzsáki, G. Single granule cells reliably discharge targets in the hippocampal CA3 network in vivo. Nat Neurosci 5, 790–795 (2002).

Hopfield JJ. Neural networks and physical systems with emergent collective computational abilities. Proc Natl Acad Sci U S A. 1982 Apr;79(8):2554-8. Doi: 10.1073/pnas.79.8.2554. PMID: 6953413; PMCID: PMC346238.

Hsieh LT, Gruber MJ, Jenkins LJ, Ranganath C. Hippocampal activity patterns carry information about objects in temporal context. Neuron. 2014 Mar 5;81(5):1165-1178. Doi: 10.1016/j.neuron.2014.01.015. PMID: 24607234; PMCID: PMC3984944.

Itskov V, Curto C, Pastalkova E, Buzsáki G. Cell assembly sequences arising from spike threshold adaptation keep track of time in the hippocampus. J Neurosci. 2011 Feb 23;31(8):2828-34. Doi: 10.1523/JNEUROSCI.3773-10.2011. PMID: 21414904; PMCID: PMC3097063.

Kraus BJ, Robinson RJ 2nd, White JA, Eichenbaum H, Hasselmo ME. Hippocampal "time cells": time versus path integration. Neuron. 2013 Jun 19;78(6):1090-101. Doi: 10.1016/j.neuron.2013.04.015. Epub 2013 May 23. PMID: 23707613; PMCID: PMC3913731.

Le Duigou C, Simonnet J, Teleñczuk MT, Fricker D, Miles R. Recurrent synapses and circuits in the CA3 region of the hippocampus: an associative network. Front Cell Neurosci. 2014 Jan 8;7:262. Doi: 10.3389/fncel.2013.00262. PMID: 24409118; PMCID: PMC3884140.

Leitner FC, Melzer S, Lütcke H, Pinna R, Seeburg PH, Helmchen F, Monyer H. Spatially segregated feedforward and feedback neurons support differential odor processing in the lateral entorhinal cortex. Nat Neurosci. 2016 Jul;19(7):935-44. Doi: 10.1038/nn.4303. Epub 2016 May 16. PMID: 27182817.

Li, X.-G., Somogyi, P., Ylinen, A., & Buzsáki, G. (1994). The hippocampal CA3 network: An in vivo intracellular labeling study. Journal of Comparative Neurology, 339(2), 181–208. https://doi.org/10.1002/cne.903390204

Lisman JE. Relating hippocampal circuitry to function: recall of memory sequences by reciprocal dentate-CA3 interactions. Neuron. 1999 Feb;22(2):233-42. doi: 10.1016/s0896-6273(00)81085-5. PMID: 10069330.

Liu D, Gu X, Zhu J, Zhang X, Han Z, Yan W, Cheng Q, Hao J, Fan H, Hou R, Chen Z, Chen Y, Li CT. Medial prefrontal activity during delay period contributes to learning of a working memory task. Science. 2014 Oct 24;346(6208):458-63. Doi: 10.1126/science.1256573. PMID: 25342800.

Lundqvist M, Herman P, Miller EK. Working Memory: Delay Activity, Yes! Persistent Activity? Maybe Not. J Neurosci. 2018 Aug 8;38(32):7013-7019. Doi: 10.1523/JNEUROSCI.2485-17.2018. PMID: 30089640; PMCID: PMC6083456.

MacDonald CJ, Lepage KQ, Eden UT, Eichenbaum H. Hippocampal "time cells" bridge the gap in memory for discontiguous events. Neuron. 2011 Aug 25;71(4):737-49. Doi: 10.1016/j.neuron.2011.07.012. PMID: 21867888; PMCID: PMC3163062.

Mayes AR, Isaac CL, Holdstock JS, Hunkin NM, Montaldi D, Downes JJ, Macdonald C, Cezayirli E, Roberts JN. Memory for single items, word pairs, and temporal order of different kinds in a patient with selective hippocampal lesions. Cogn Neuropsychol. 2001 Mar 1;18(2):97-123. Doi: 10.1080/02643290125897. PMID: 20945208.

Middleton SJ, McHugh TJ. Silencing CA3 disrupts temporal coding in the CA1 ensemble. Nat Neurosci. 2016 Jul;19(7):945-51. Doi: 10.1038/nn.4311. Epub 2016 May 30. PMID: 27239937.

Miles, R., & Wong, R. K. (1987). Inhibitory control of local excitatory circuits in the guinea-pig hippocampus. The Journal of Physiology, 388(1), 611–629. https://doi.org/10.1113/jphysiol.1987.sp016634

Modi MN, Dhawale AK, Bhalla US. CA1 cell activity sequences emerge after reorganization of network correlation structure during associative learning. Elife. 2014 Mar 25;3:e01982. Doi: 10.7554/eLife.01982. PMID: 24668171; PMCID: PMC3964823.

Nakashiba, T., Buhl, D. L., McHugh, T. J., & Tonegawa, S. (2009). Hippocampal CA3 output is crucial for ripple-associated reactivation and consolidation of memory. Neuron, 62(6), 781–787. https://doi.org/10.1016/j.neuron.2009.05.013

Nakashiba, T., Young, J. Z., McHugh, T. J., Buhl, D. L., & Tonegawa, S. (2008). Transgenic inhibition of synaptic transmission reveals role of CA3 output in hippocampal learning. Science, 319(5867), 1260–1264. https://doi.org/10.1126/science.1151120

Naya Y, Suzuki WA. Integrating what and when across the primate medial temporal lobe. Science. 2011 Aug 5;333(6043):773-6. Doi: 10.1126/science.1206773. PMID: 21817056.

Pastalkova E, Itskov V, Amarasingham A, Buzsáki G. Internally generated cell assembly sequences in the rat hippocampus. Science. 2008 Sep 5;321(5894):1322-7. Doi: 10.1126/science.1159775. PMID: 18772431; PMCID: PMC2570043.

Rebola N, Carta M, Mulle C. Operation and plasticity of hippocampal CA3 circuits: implications for memory encoding. Nat Rev Neurosci. 2017 Apr;18(4):208-220. Doi: 10.1038/nrn.2017.10. Epub 2017 Mar 2. PMID: 28251990.

Remaud J, Ceccom J, Carponcy J, Dugué L, Menchon G, Pech S, Halley H, Francés B, Dahan L. Anisomycin injection in area CA3 of the hippocampus impairs both short-term and long-term memories of contextual fear. Learn Mem. 2014 May 15;21(6):311-5. Doi: 10.1101/lm.033969.113. PMID: 25171422; PMCID: PMC4024620.

Rolls ET. A quantitative theory of the functions of the hippocampal CA3 network in memory. Front Cell Neurosci. 2013 Jun 25;7:98. Doi: 10.3389/fncel.2013.00098. PMID: 23805074; PMCID: PMC3691555.

Salz DM, Tiganj Z, Khasnabish S, Kohley A, Sheehan D, Howard MW, Eichenbaum H. Time Cells in Hippocampal Area CA3. J Neurosci. 2016 Jul 13;36(28):7476-84. Doi: 10.1523/JNEUROSCI.0087-16.2016. PMID: 27413157; PMCID: PMC4945667.

Scoville WB, Milner B. Loss of recent memory after bilateral hippocampal lesions. J Neurol Neurosurg Psychiatry. 1957;20(1):11-21. Doi:10.1136/jnnp.20.1.11

Sun, Y., Nguyen, A. Q., Nguyen, J. P., Le, L., Saur, D., Choi, J., Callaway, E. M., & Xu, X. (2014). Cell-type-specific circuit connectivity of hippocampal CA1 revealed through Cre-dependent rabies tracing. Cell Reports, 7(1), 269–280.

Taxidis J, Pnevmatikakis EA, Dorian CC, Mylavarapu AL, Arora JS, Samadian KD, Hoffberg EA, Golshani P. Differential Emergence and Stability of Sensory and Temporal Representations in Context-Specific Hippocampal Sequences. Neuron. 2020 Dec 9;108(5):984-998.e9. doi: 10.1016/j.neuron.2020.08.028. Epub 2020 Sep 18. PMID: 32949502; PMCID: PMC7736335.

Treves A, Rolls ET. Computational constraints suggest the need for two distinct input systems to the hippocampal CA3 network. Hippocampus. 1992 Apr;2(2):189-99. Doi: 10.1002/hipo.450020209. PMID: 1308182.

Tulving E. 1972. Episodic and semantic memory. In Organization of Memory, ed. E Tulving, W Donaldson, pp. 381– 403. New York: Academic

Xu W, Wilson DA. Odor-evoked activity in the mouse lateral entorhinal cortex. Neuroscience. 2012 Oct 25;223:12-20. doi: 10.1016/j.neuroscience.2012.07.067. Epub 2012 Aug 4. PMID: 22871522; PMCID: PMC3455128.

Zhang X, Yan W, Wang W, Fan H, Hou R, Chen Y, Chen Z, Ge C, Duan S, Compte A, Li CT. Active information maintenance in working memory by a sensory cortex. Elife. 2019 Jun 24;8:e43191. doi: 10.7554/eLife.43191. PMID: 31232695; PMCID: PMC6634975.

Chapter 2

Sequential activity in CA3

2.1 INTRODUCTION

Two subsets of cells emerge from CA1 pyramidal neurons during an olfactory-modified working memory task: odor cells and odor-specific time cells (Taxidis et al., 2020). Odor cells are active at the presentation of odors, encoding olfactory cues. Odor cells are reliably activated across nearly all trials of the task. Odor-specific time cells are active during the delay period and encode odor-specific time points. Each odor triggers a specific sequence of time cell firing that tiles the delay (Taxidis et al., 2020).

It is not known if odor cells and odor-specific time cells exist in CA3 during an olfactory modified working memory task; these cells have never before been imaged during this task. Confirming the existence of odor and odor-specific time cells that fire sequentially would prove that CA3 contains populations of cells that respond selectively to a sensory stimulus and others that fire in a stimulus-specific sequence in the delay following the stimulus. This would indicate that CA3 neurons process sensory and temporal information.

2.2 CA3 CELLS ENCODE TIME AND ODOR INFORMATION

To understand how CA3 works, we must selectively express calcium indicators in CA3 neurons. This is an especially difficult problem for CA3 due to its anatomy. CA3 lies along the curve of hippocampus. CA2 is a small subregion next to, and slightly on top of, CA3. Previous CA3 imaging studies also likely imaged CA2 neurons as the virus likely spread to CA2. since the imaging window lies above both CA2 and CA3. Given these circumstances, is impossible to distinguish between CA2 and CA3 cells. To solve this problem, we used the Tg(Grik4-cre)G32-4Stl line (Jackson strain stock #006474). In this transgenic line, the transcriptional regulatory region of the KA-1 gene drives expression of the *Cre* transgene. KA-1 is robustly expressed in the CA3 pyramidal layer. Transgene expression (*Cre* activity) is detectable at 14 days old in CA3, and at 8 weeks recombination is observed in nearly 100% of pyramidal cells in CA3 (Nakazawa et al., 2002). Therefore, only excitatory cells in CA3 will express *Cre*. The Girk4Cre mice received a unilateral CA3 injection of AAV1-syn-FLEX-jGCaMP7f-WPE, to express GCAMP7f, a green-fluorescent calcium indicator (**Fig. 2.1**). Since the expression of GCaMP7f is Cre-dependent, GCaMP7f will only express in CA3 cells. Using this intersectional method, we can know with certainty that the cells we are imaging are CA3 excitatory neurons.

We performed *in vivo* two-photon calcium imaging as a proxy for recording action potential firing from large populations of CA3 neurons. A 3-mm diameter cranial window was implanted over CA3. Following surgery, mice were trained to perform a modified odor-based delayed non-match-to-sample (DNMS) working memory task (Zhang et al., 2019; Lui et al.,

2014) In this task, mice were presented two odors with a five-second delay between odors. Mice were taught to lick when the odors differ and withhold licking when the odors were the same. Mice must hold the memory of the first odor for five seconds and compare it with the second odor to give the correct response (Fig. 2.2). Mice received a water reward for correct responses. Training was split into three shaping steps: (1) Day 7-9: habituation to the behavioral rig. (2) Day 10-13: Lick shaping, in which mice learned to lick after the presentation of two odors separated by a 5 second delay. (3) Day 14-24: non-match-to-sample shaping, in which mice learned to correctly reject match odor trials and lick for non-match odor trials (Fig. 2.3) (Expanded surgical and behavioral training procedures can be found in the 2.7 Methods section.). Water deprivation began with the first day of habituation (day 7), the first shaping step of the DNMS task training.

Two-photon calcium imaging began on the first day of the third shaping step (day 14), non-match-to-sample shaping. Blood vessel patterns and precise alignment of the animal were utilized to image the same set of neurons each day. The odors presented and licking responses of the animals, synchronized to the calcium imaging data, were recorded. Mice underwent 8-12 sessions of 20 trials each per day. During the first few days of imaging, mice learned to only lick during non-match odor trials. Mice learned quickly and soon consistently performed above 80% accuracy (Fig. 2.4). There was a small dip in performance during day seven. This dip could have been caused by slight changes in the environment that affected mice performance. In our analysis, we delineated sessions according to performance, with sessions above 85% labeled as well-trained sessions.

A schema of the experimental set-up for two-photon calcium imaging during the DNMS task can be seen in Fig. 2.5. An example of the imaging plane can be seen in Fig. 2.6A. CA3 cells was seen as a strip of cells. The cranial window was centered on CA3 (Fig. 2.5). Since the image was viewed from the dorsal side of the hippocampus, the curve of CA3 was cut into stripes in the imaging plane (Fig. 2.6A). We imaged with a resonant two-photon Scientifica microscope and 16x 0.8 NA Nikon objective at 920 nm. We recorded at 30.9 Hz, 512 x 512 pixel frames, and an average power of 118.5 mW. This produced a 500x500 μm field of view.

The calcium imaging data analysis pipeline Suite2p (Pachitariu et al., 2017) was first used for alignment, motion correction, and ROI detection (Fig. 2.6B). The fluorescence of the neuropil was subtracted from the fluorescence of the cell for better signal detection. Then the trace was then passed through a 3 Hz low-pass filter script that we custom wrote (Supplementary Fig. 2.1). The data was then passed through Suite 2P's deconvolution script. Each trace was deconvolved to remove the slow decay of calcium transients and used to calculate estimated cell activity. Deconvolution was based on the OASIS algorithm (Friedrich et al., 2017) (Fig. 2.7) and run with only a non-negativity constraint. Deconvolution of calcium transients is only an estimate of cell activity, not a true measure of cell firing, but was used here as a proxy for cell activity.

Responses of CA3 neurons during the task were highly diverse. Some CA3 neurons were active during either odor presentation or at specific time points in the delay. Other CA3 neurons were active only after presentation of one odor and not the other and were therefore odor-specific (Fig. 2.8A. top graphs). Other CA3 neurons fired during the delay period only after a specific odor and could be classified as CA3 odor-specific time cells. These cells were active during most trials that began with a specific odor and were only active during a consistent time window during the delay period (Fig. 2.9A. top graphs). To test if the cells were encoding odor and temporal information, we used Monte-Carlo simulations to determine whether the peak activity of neurons was greater than chance. Chance levels of activity were determined by circularly shuffling the cell activity in each trial 500 times. We took the max of the mean activity across trials in each of the 500 shuffles and created a distribution. Activity that exceeded the 99th percentile of this distribution was deemed significant. An odor cell was defined as a cell that had its maximal mean activity above this threshold during the one second odor 1 presentation window (Fig. 2.8. bottom graphs). An odor-specific time cell was defined as a cell that had its maximal mean activity above the threshold during the five second delay period following odor 1 presentation (Fig. 2.9. bottom graphs). A cell with maximal mean activity above threshold during odor A presentation was called an 'odor A cell'. A cell with maximal mean activity above threshold during the delay period following odor A presentation was called a 'time A cell'. This was similarly defined for cells specific to odor B. With these definitions, we found both CA3 odor-specific cells and CA3 odor-specific time cells (Fig. 2.8 and Fig. 2.9) within the CA3 cell population. This finding shows that CA3 does indeed encode odor and temporal information.

Figure 2.1.

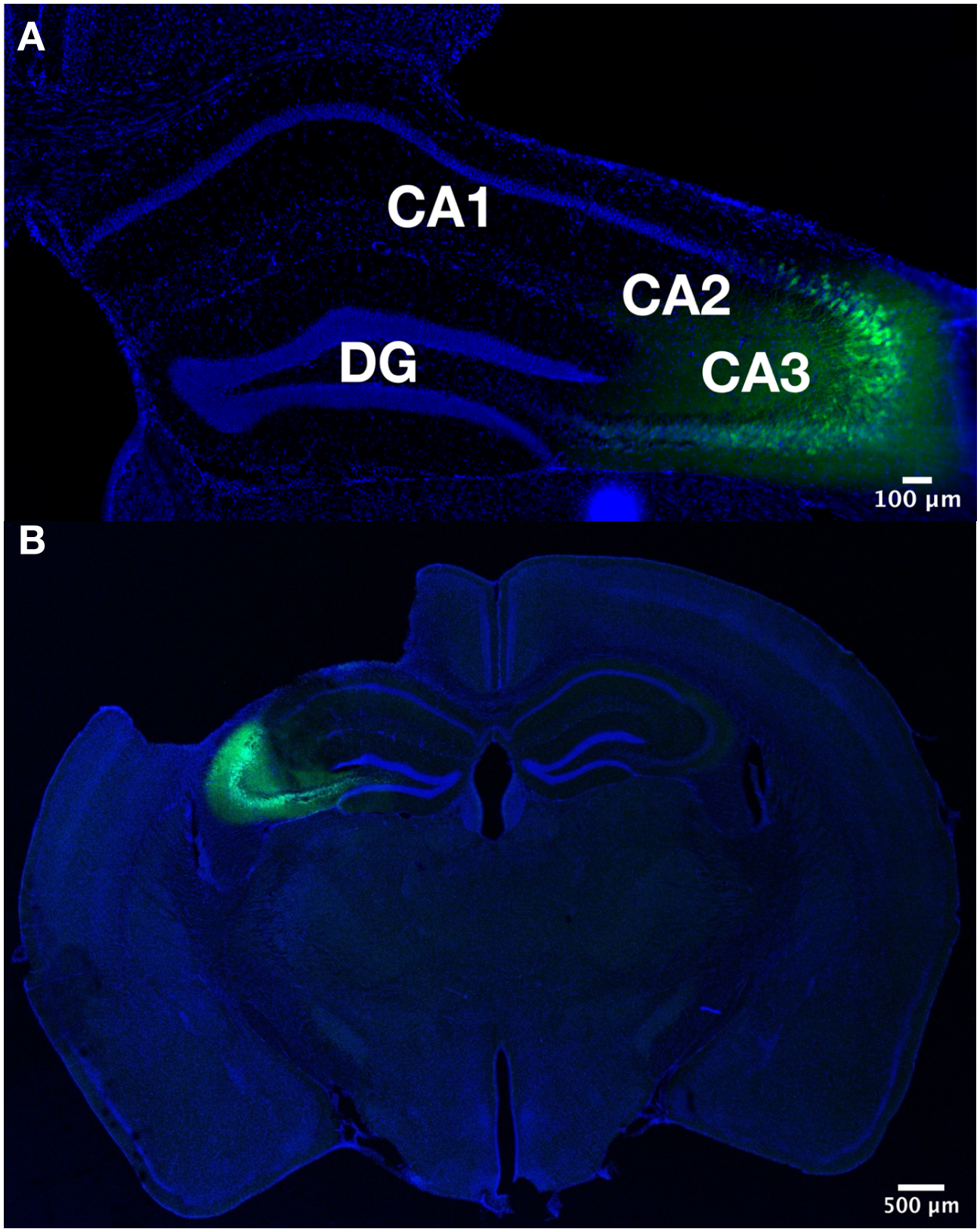

Figure 2.1. CA3 viral targeting in Girk4Cre mice. GCaMP7f is in green. DAPI is in blue. (A) 10x image of the hippocampus showing viral injection targeting of CA3. (B) 5x image of a coronal brain slice showing viral injection targeting of CA3 and placement of the cranial window above CA3.

Figure 2.2.

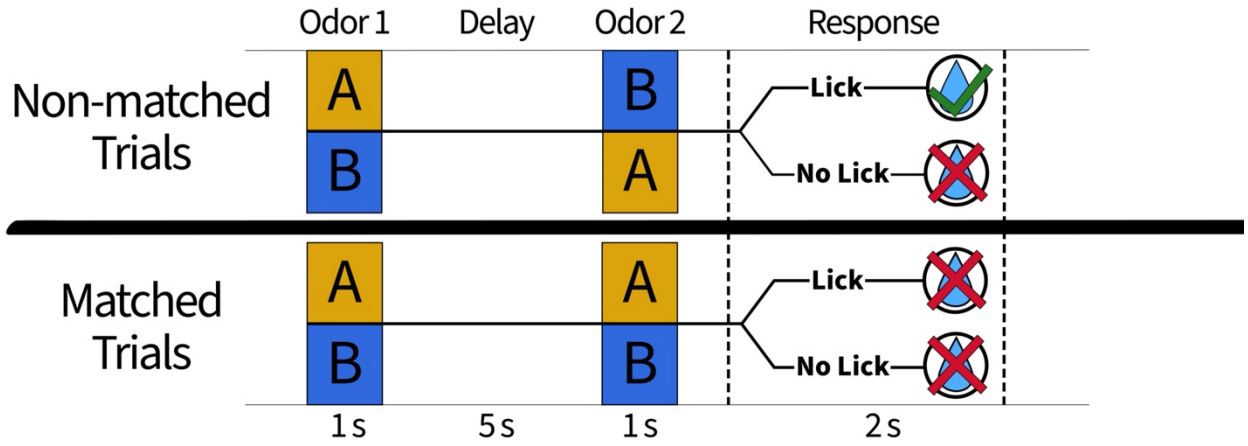

Figure 2.2. Odor-based Delayed Non-Match-to-Sample task. Mice were presented two odors (odor A in yellow or odor B in blue) with a five-second delay in between. Mice were rewarded for licking in response to non-match odor trials.

Figure 2.3.

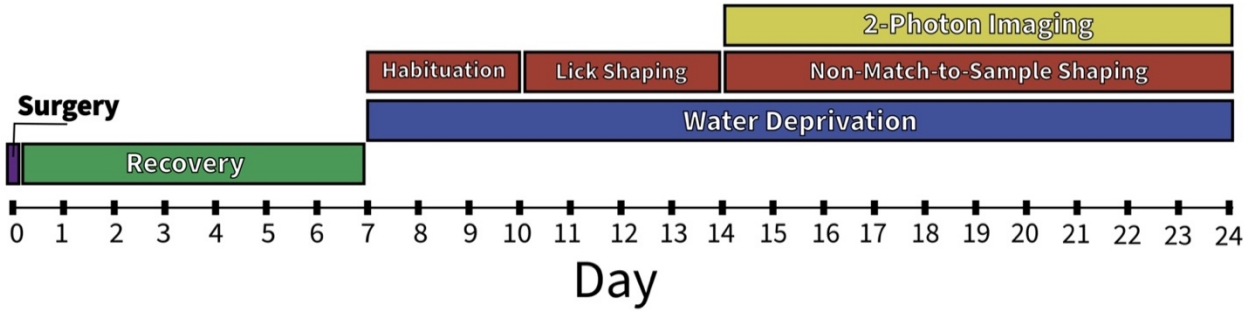

Figure 2.3. Behavioral training timeline. DNMS task training (red boxes) was split into (1) habituation, (2) lick shaping, and (3) non-match-to-sample shaping. Two-photon imaging began in the third step of the DNMS task training. Water deprivation began at the first step of the DNMS task training.

Figure 2.4.

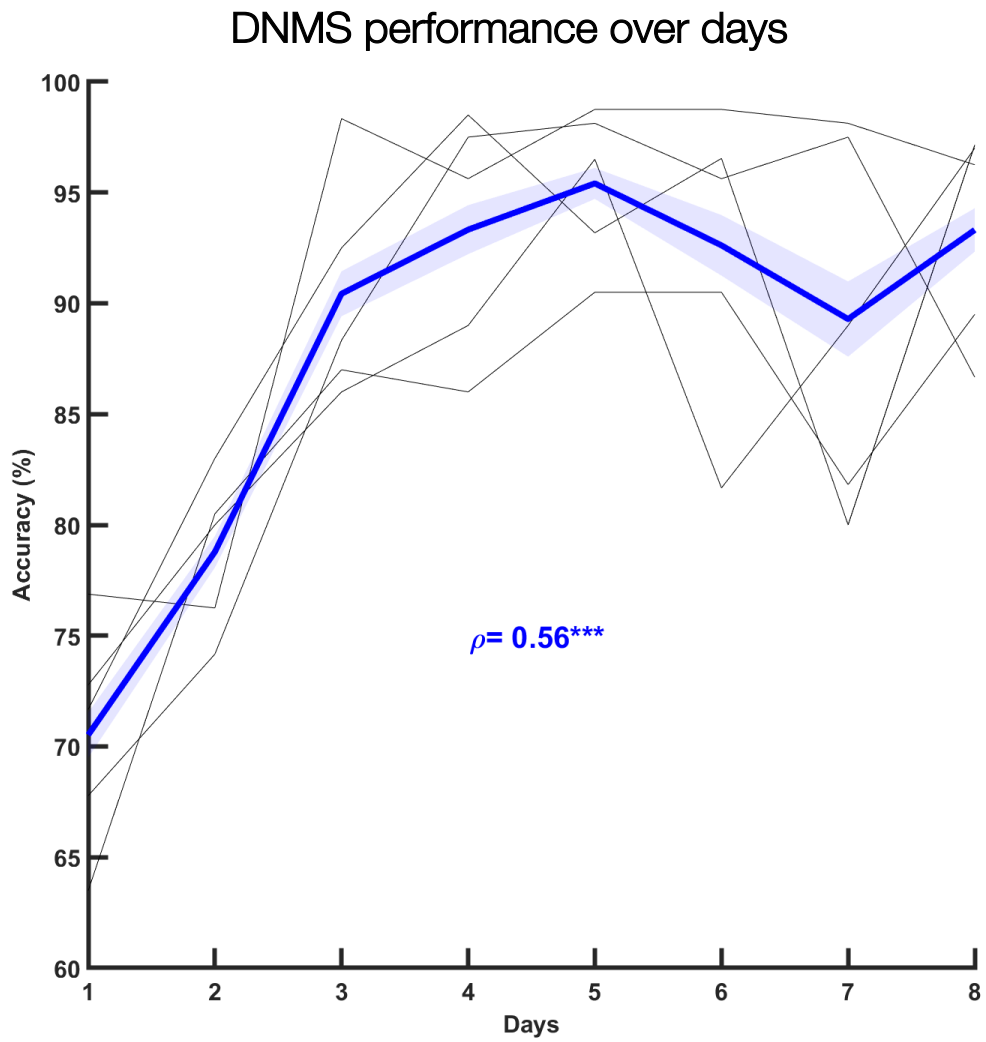

Figure 2.4. DNMS performance over days. Performance in the DNMS task over days, starting with day 1 of the non-match-to-sample shaping (step 3 of the DNMS training). Two-photon calcium imaging began on day 1. Each grey line represents the performance of one mouse (n = 5). The blue line is the averaged performance over all mice ($\rho = 0.53$). The shaded blue region is the standard error. *** $p < 0.01$.

Figure 2.5.

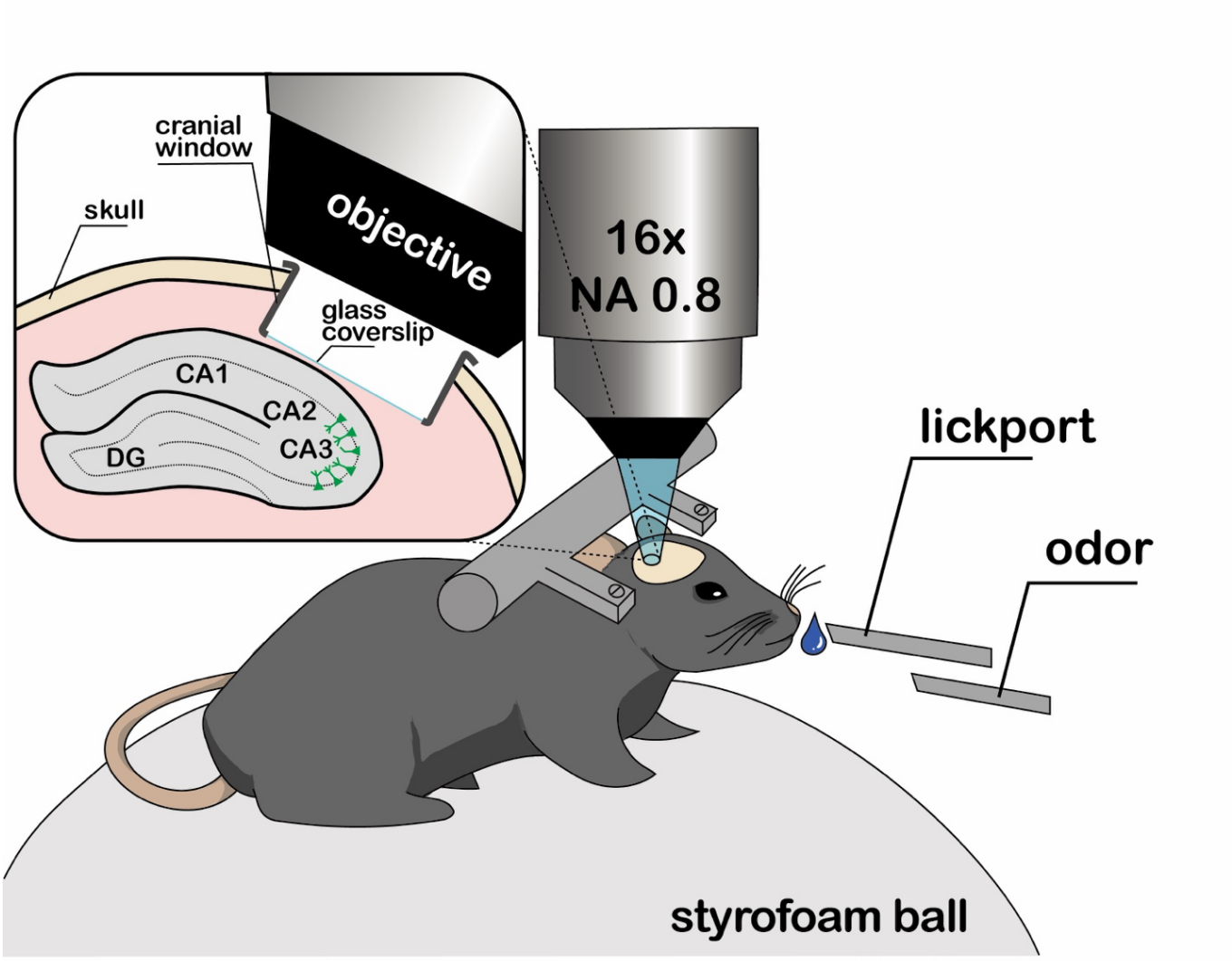

Figure 2.5. Experimental schema. Mouse performing the DNMS task during *in vivo* two-photon calcium imaging. A 16x, NA 0.8 water-immersion objective was utilized. The cranial window sat over CA3. Water droplets were delivered through a lick port. Odors were delivered through a separate port. The mouse was freely running on a Styrofoam ball.

Figure 2.6.

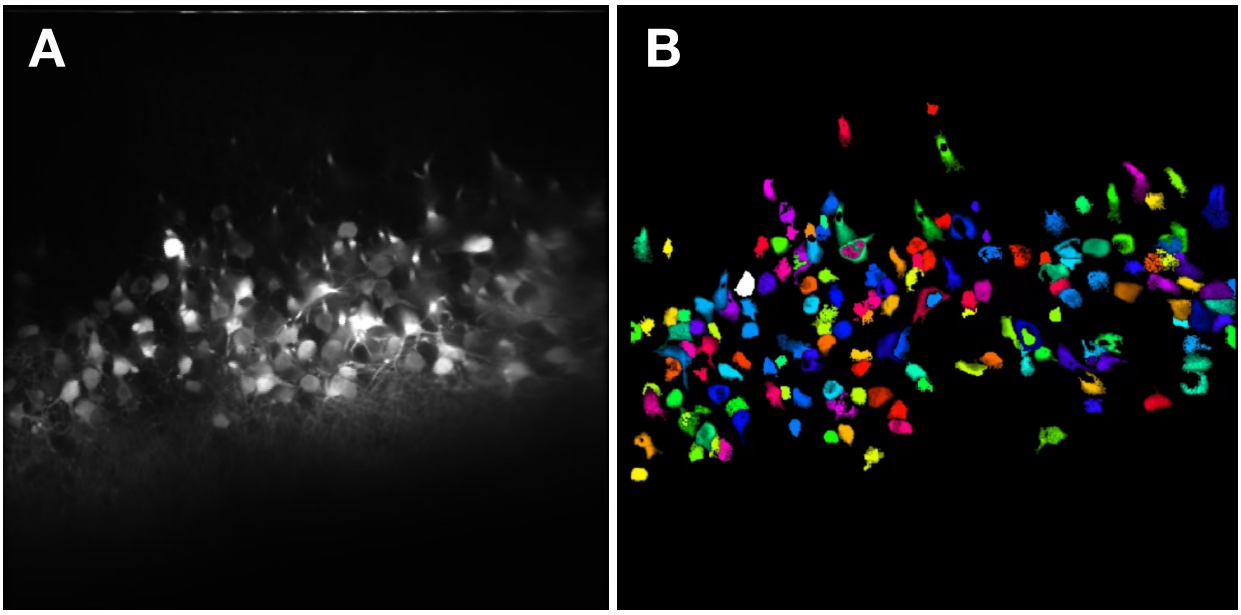

Figure 2.6. CA3 two-photon imaging plane. (A) Averaged raw two-photon image of CA3. (B) ROIs detected through Suite2p.

Figure 2.7.

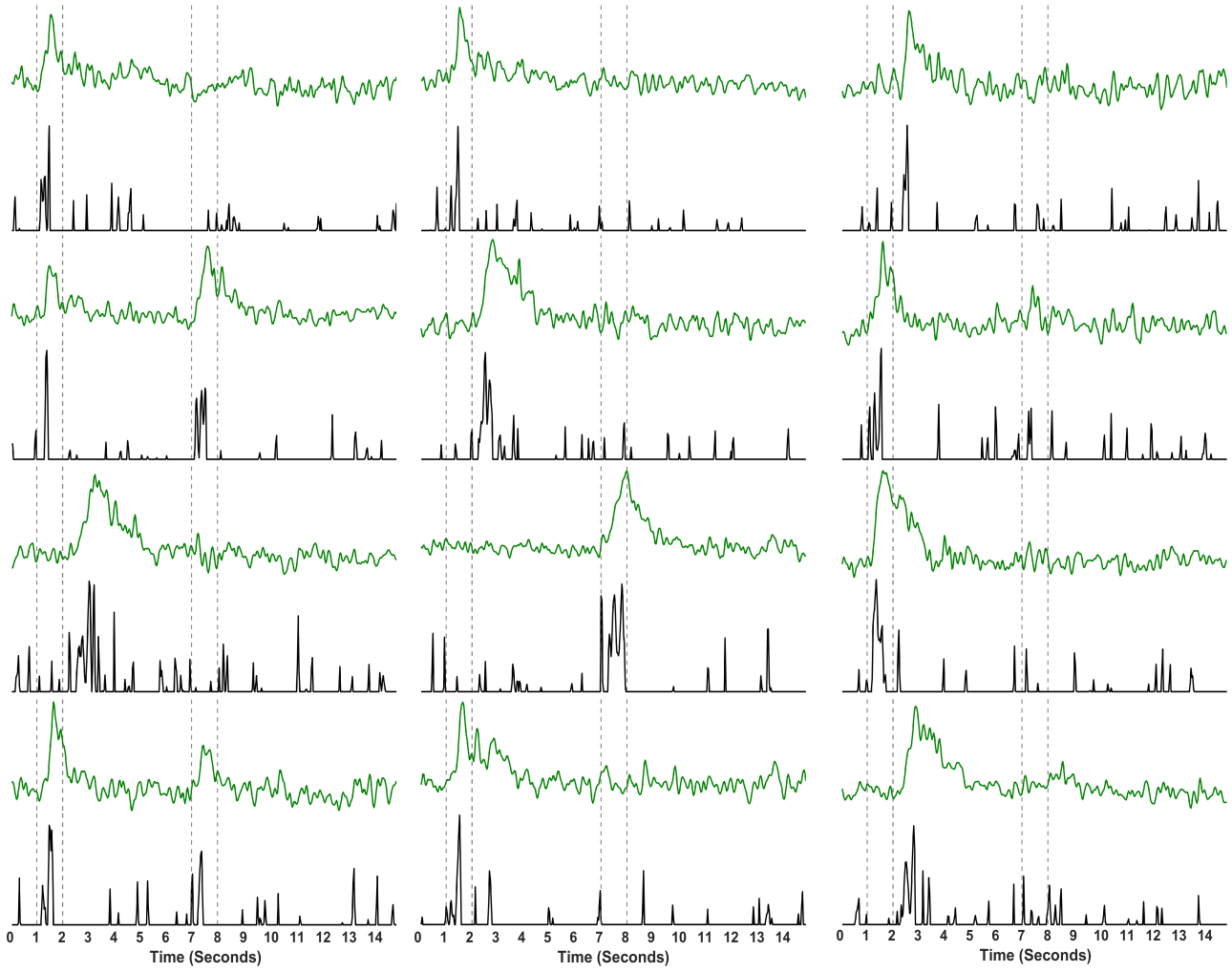

Figure 2.7. Examples of deconvolution. Each graph is the activity of one cell over one trial. The fluorescence of the cell subtracted by the fluorescence of the neuropil is in green. The deconvolved estimated cell activity is in black. The dotted lines denote the 1 second odor presentations.

Figure 2.8.

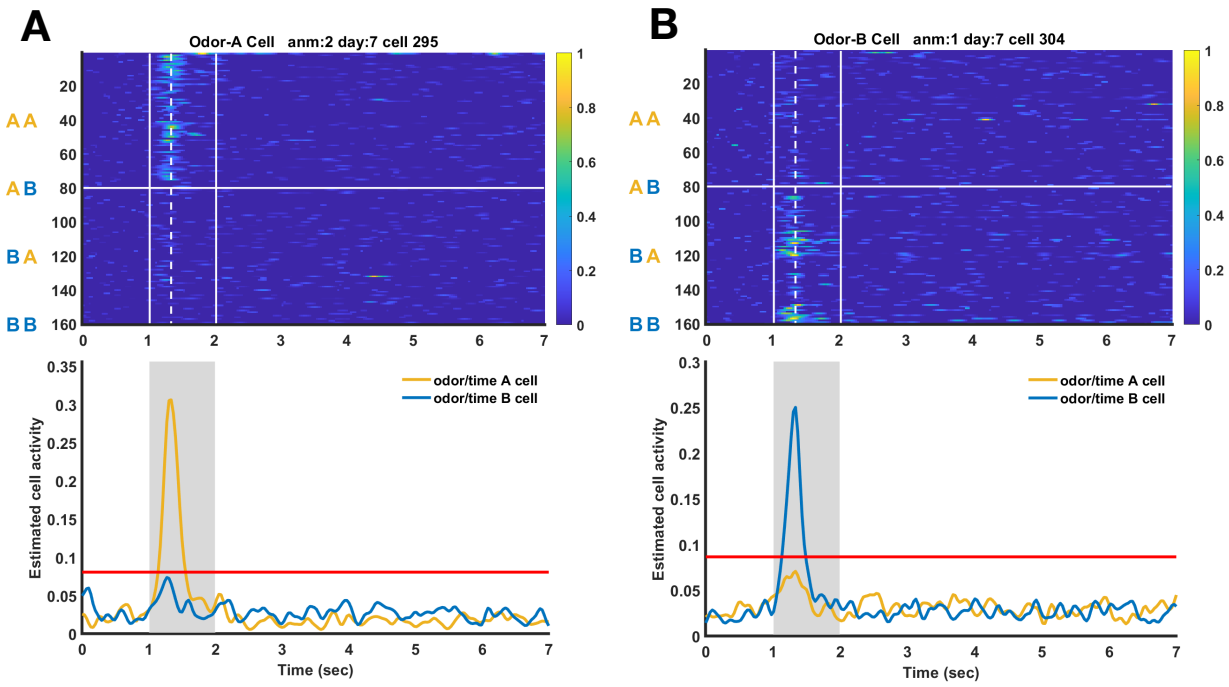

Figure 2.8. Examples of CA3 odor cells. (A) Example of a CA3 odor A cell. The odor A cell was mostly active during odor 1 presentation in trials that began with odor A (AA, AB). The top graph is a heatmap of the normalized estimated activity of one cell across 160 trials. Each row is one trial. The trials are split into the four possible odor presentation combinations (AA, AB, BA, BB). The solid white horizontal line separate trials that began with odor A from trials that began with odor B. The solid white vertical lines denote the 1-second odor 1 presentation. The dotted white vertical line marks the max mean activity of the cell across all trials. The bottom graph is the mean estimated normalized cell activity across all trials. Odor A is in yellow. Odor B is in blue. The red horizontal line is the threshold for significant activity. The shaded grey region denotes the 1-second odor 1 presentation. (B) Example of a CA3 odor B cell. The odor B cell was mostly active during odor 1 presentation in trials that begin with odor B (BA, BB). The top and bottom graph are as described in (A).

Figure 2.9.

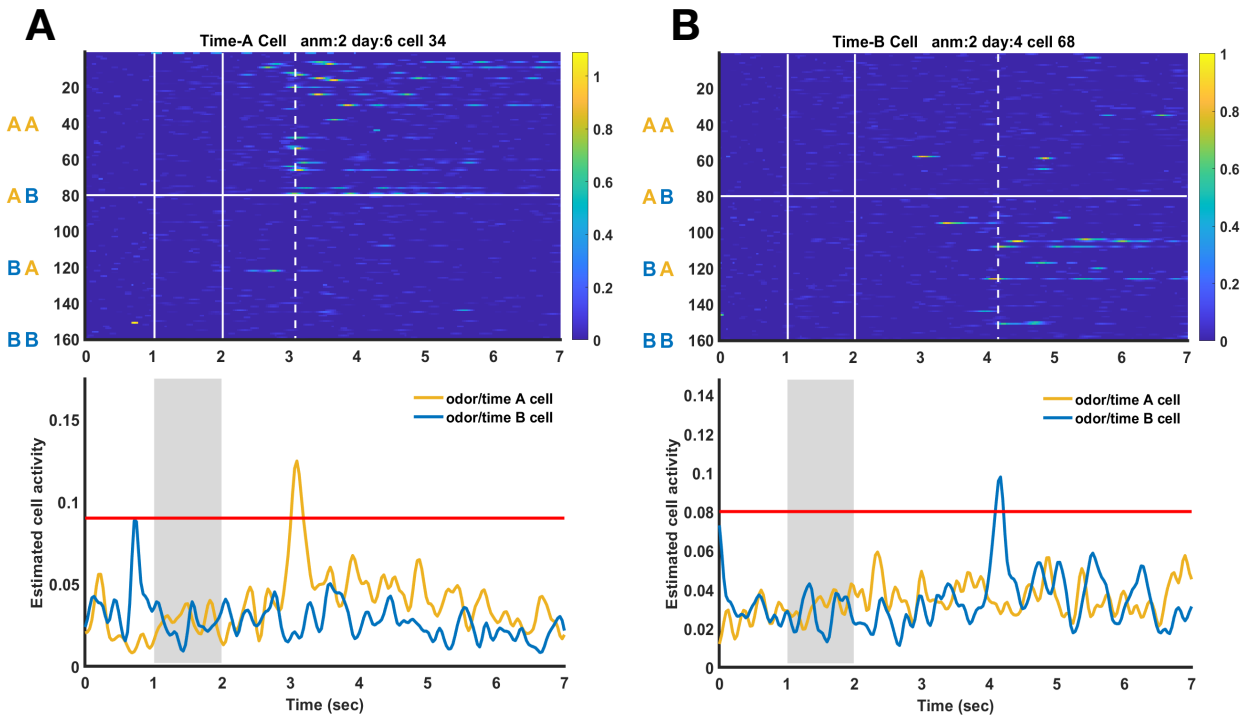

Figure 2.9. Examples of CA3 odor-specific time cells. (A) Example of a CA3 time A cell. The time A cell was mostly active around second 3 of the delay in trials that began with odor A (AA, AB). The top graph is a heatmap of the normalized estimated activity of one cell across 160 trials. Each row is one trial. The trials are split into the four possible odor presentation combinations (AA, AB, BA, BB). The solid white horizontal line separate trials that began with odor A from trials that began with odor B. The solid white vertical lines denote the 1-second odor 1 presentation. The dotted white vertical line marks the max mean activity of the cell across all trials. The bottom graph is the mean estimated normalized cell activity across all trials. Odor A is in yellow. Odor B is in blue. The red horizontal line is threshold for significant activity. The shaded grey region denotes the 1-second odor 1 presentation. (B) Example of a CA3 odor B time cell. The time B cell was mostly active around second 4 of the delay in trials that began with odor B (BA, BB). The top and bottom graph are as described in (A).

2.3 SEQUENTIAL ACTIVITY IN CA3

We have shown that CA3 encodes odor and temporal on an individual cell level. What does the activity of the CA3 cell population look like as whole? Does CA3 display the same sequential activity that has been found in CA1? We took the mean estimated activity of each significant cell, as defined in the previous section, and sorted the cells by the time-bin of their maximal mean activity. We saw sequential activity for both odor-A and odor-B specific significant cells. Odor-specific cells fired sequentially beginning at first odor presentation and tiled the entire delay (Fig. 2.10). Sequences were odor specific. When odor A sequence cells activity was plotted during odor B trials, sequential activity was abolished, though many odor cells and time cells can be seen to fire to both odors. (Fig. 2.11B) This was similarly true for odor B sequences cells plotted during odor A trials (Fig. 2.11F) A larger percent of the odor cell population was active during the early odor presentation time-bins compared to later odor presentation time-bins (Fig. 2.10C). A larger percent of the time cell population was active within the first second of the delay compared to later delay time-bins (Fig.2.10C). Each animal (n = 5) had on average 3000 cells pooled across all days. Odor A cells represented 4.15% ± 0.59 of the cell population, time A cells represented 2.53% ± 0.36 of the cell population, odor B cells represented 4.76% ± 0.67 of the cell population, time B cells represented 1.53% ± 0.23 of the cell population (Fig. 2.10D).

Since sorting of randomly generated traces will appear to show sequential activity, we used cross-validation methods to ensure that the sequential activity we demonstrated was not an artifact of the sorting method. To validate the sequential activity, we took the odd trials and

sorted by the time-bin of each cell's maximal mean activity. This created the sequential activity that was seen when all trials were sorted. We then took the order of the odor trials and implemented it on the even trials. We saw that the sequential activity was still present in the even trials that had been sorted by odd trials (Fig. 2.11 C, G). This was true for both odor A and odor B sequence cells. We also compared the correlation of even and odd trials to a shuffled baseline. For odor A sequence cells and odor B sequence cells, there was a significant difference from the shuffled baseline (odor A: $p = 4.02e-221$, odor B: $p = 7.9312e-101$) (Fig. 2.11 D, H). This meant that the odd and even trials were more similar to each other than compared to chance. These results show that the CA3 sequential activity is not an artifact of sorting. Though CA3 sequential activity was found and validated as described above in each mouse, there was variability in how the sequential activity looked (Supplementary Fig. 2.2, 2.3) and how many time cells there were.

Figure 2.10.

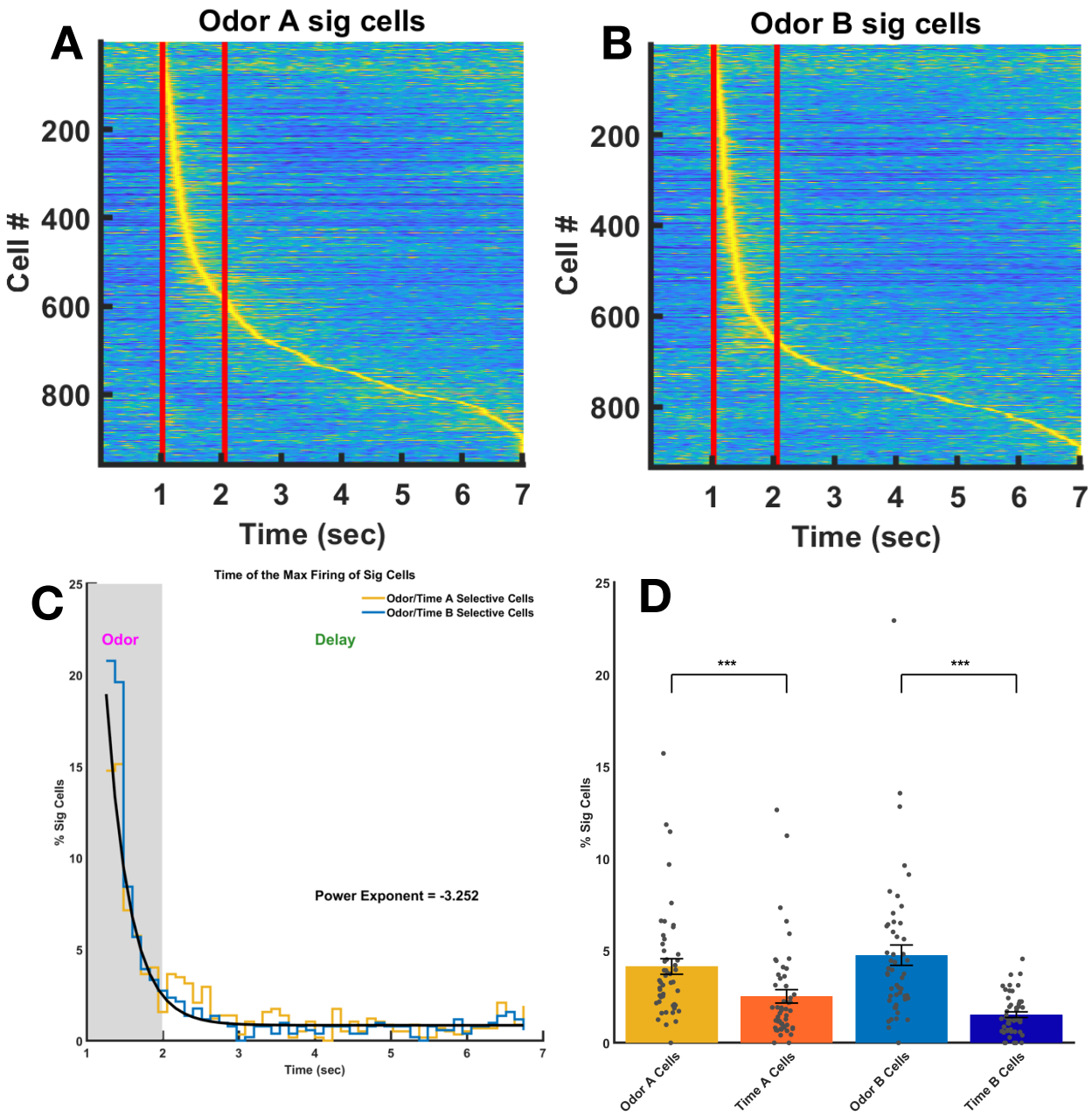

Figure 2.10. CA3 sequential activity. (A) Activity heatmap of CA3 odor A cells and odor A time cells sorted by the time-bin of maximal mean activity. Cells are pooled across all animals (n = 5) and all days (n = 50). (B) Activity heatmap of CA3 odor B cells and odor B time cells sorted by the time-bin of maximal mean activity. Cells are pool across all animals (n = 5) and all days (n = 50). Each row represents the normalized mean activity across trials of one cell. The red lines denote the one second odor 1 presentation time-bin. (C) Time-bin of maximal firing of significant cells. Yellow line is for odor A specific cells. Blue line is for odor B specific cells. Black line for all significant cells. The shaded grey area denotes the odor presentation window. The power exponent is -3.252. (D) Breakdown of CA3 significant cells (n = 2443 ±

498.47): Odor A cells (4.15% ± 0.59), odor A-specific time A cells (2.53% ± 0.36), odor B cells (4.76% ± 0.67), odor B-specific time B cells (1.53% ± 0.23). ***ρ <0.001.

Figure 2.11.

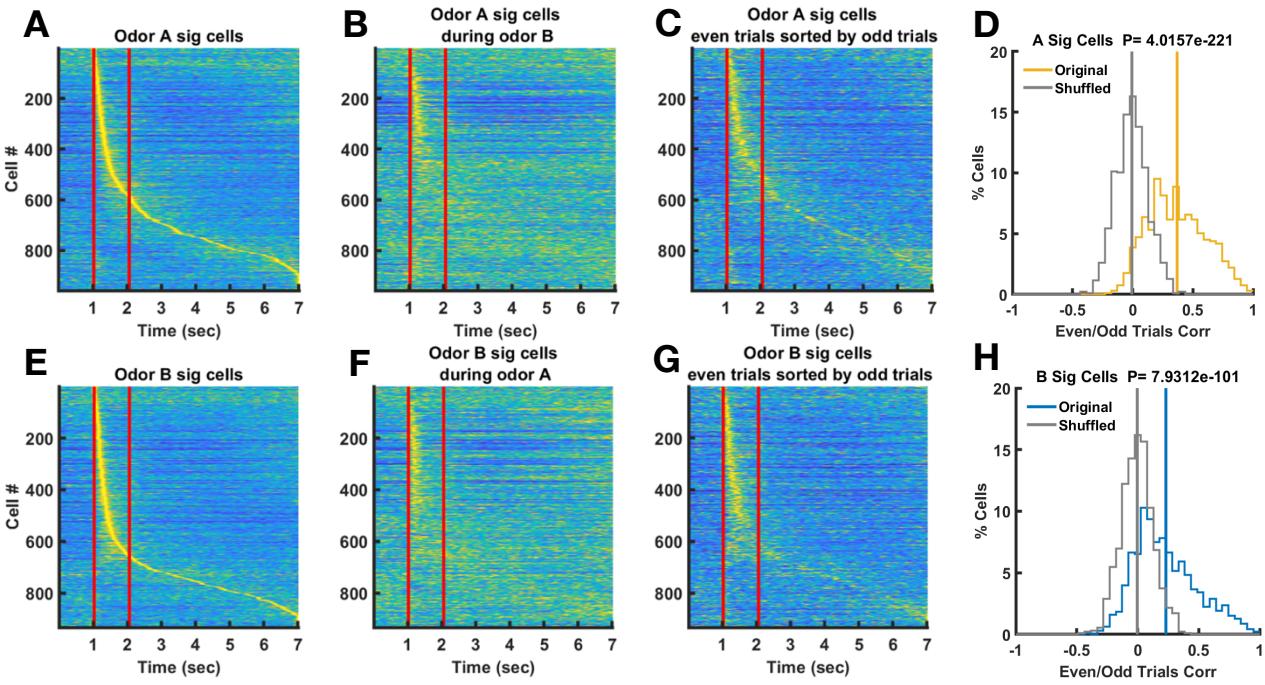

Figure 2.11. CA3 sequential activity validation. Cells are pooled across all animals and days (n = 2443 ± 498.47). (A) Odor A cells during odor A trials, sorted by each cell's maximal average activity. Sequential activity is present. (B) Odor A cells during odor B trials. Sequential activity is absent. (C) Odor A cells during even odor A trials, sorted by odd odor A trials. Sequential activity is still present. (D) Correlation between even and odd odor A trials (p = 4.02e-221). (E) Odor B cells during odor B trials. Sequential activity is present. (F) Odor B cells during odor A trials. Sequential activity is absent. (G) Odor B cells during even odor B trials, sorted by odd odor B trials. Sequential activity is still present. (H) Correlation between even and odd odor B trials (p = 7.93e-101).

2.4 LOW SELECTIVITY IN CA3 CELL POPULATION

After confirming that CA3 cells encode sensory and temporal information and fire in a sequential manner, we wanted to further investigate the unique properties of these cells. Since the sequence cells fire to specific odors, we tested the strength of this odor preference. To do this, we calculated the odor selectivity index (SI) for each cell with significant activity, as defined in previous sections. Odor selectivity index was calculated as the ratio of $(R_{pref} - R_{nonpref})/(R_{pref} + R_{nonpref})$. R_{pref} is the estimated mean activity at the single time-bin of the cell's maximal mean activity during preferred odor trials. $R_{nonpref}$ is the estimated mean activity at that same time-bin, but in the non-preferred odor trials. The odor SI is a ratio that describes how much one odor is preferred over the other. The stronger the preference is, the closer the ratio is to one. The weaker the preference is, the closer the ratio is to zero.

The CA3 cells have low selectivity indexes across all cell subgroups (Odor A cells: mean SI 0.28; Time A cells: mean SI 0.36; Odor B cells: mean SI 0.28; Time B cells: mean SI 0.36) (Fig. 2.12). This means that while the majority of CA3 cells display odor preference, that preference was very small, since the odor SI were close to zero. This finding was surprising, so re-examined all CA3 cells to confirm the presence of non-selective cells. We were able to identify both non-selective CA3 odor and time cells (Fig. 2.13). CA3 cell low odor selectivity contrasts with the high odor selectivity recorded in CA1 (Taxidis et al., 2020).

We were curious if CA3 odor selectivity stayed consistent across time. Was there stronger odor preference at the beginning of the trial during the odor presentation and this preference weakened towards the end of the delay? We graphed the odor SI of CA3 significant cells according to the time-bin of their average maximal activity. We found that the odor SI stayed relatively constant across time (Pearson correlation, $\rho = 0.17$; $p = 0.65$) (**Fig. 2.14A**). Mean odor SI for odor cells was 0.402 ± 0.010. Mean odor SI for time cells was 0.396 ± 0.008. There was no significant difference between the mean odor SI of odor cells and time cells ($p = 0.63$) (**Fig. 2.14B**), meaning that there was no significant difference in the strength of odor preference between cells that were significantly active during odor presentation and those significantly active during the delay. CA1 cell odor SI was also stayed constant across time (Taxidis et al., 2020).

Figure 2.12

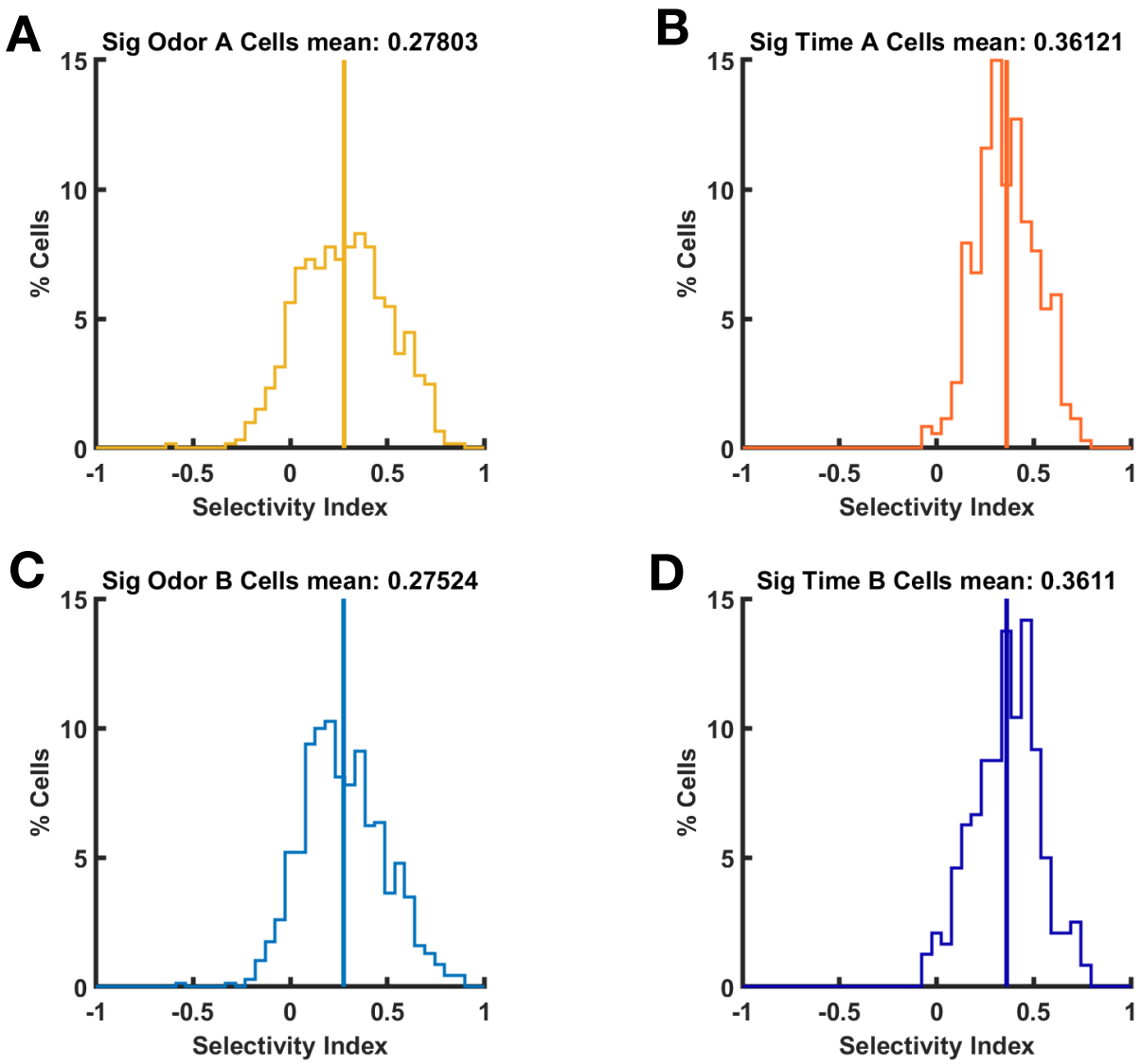

Figure 2.12. Low selectivity across all CA3 cells. Distribution of selectivity index (SI) in (A) Odor A cells (mean = 0.28), (B) Time A cells (mean = 0.36), (C) Odor B cells (mean = 0.28), (D) Time B cells (mean = 0.36).

Figure 2.13.

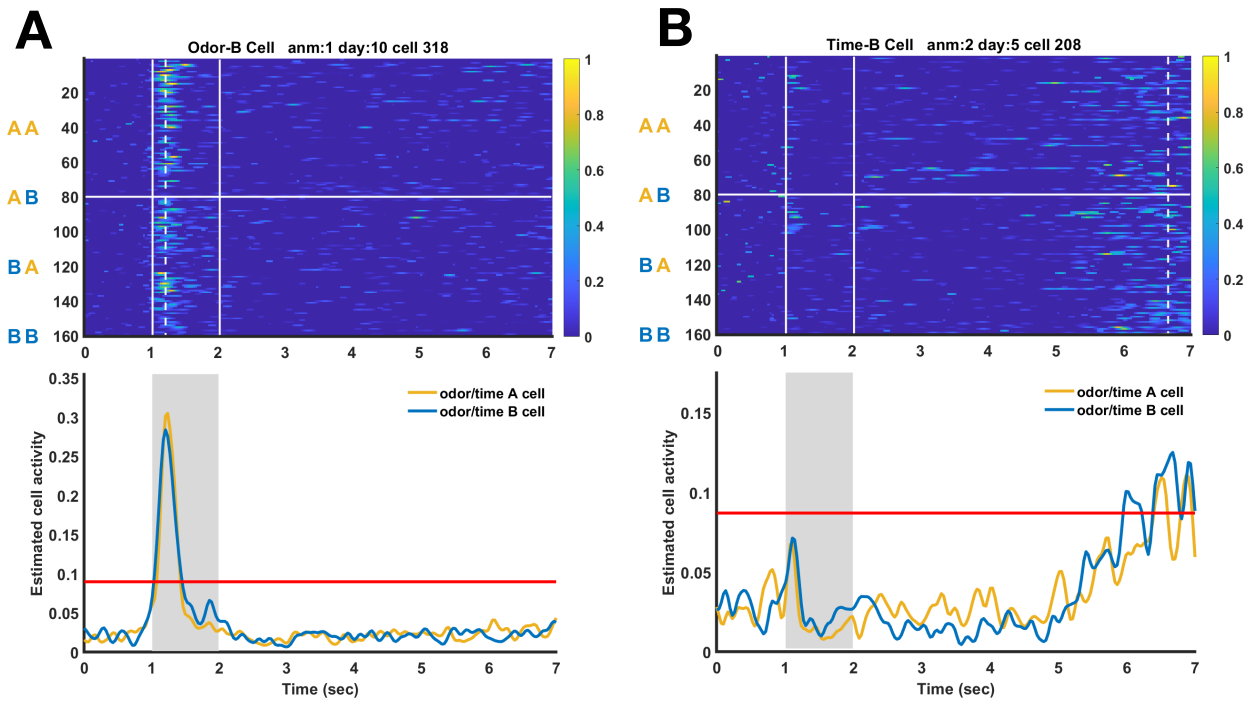

Figure 2.13. CA3 non-selective cells. (A) Example of a CA3 non-selective odor cell. (B) Example of a CA3 non-selective time cell. The top graph is a heatmap of the normalized estimated activity of one cell across 160 trials. Each row is one trial. The trials are split up into the four possible odor presentation combinations (AA, AB, BA, BB). The solid white horizontal line separate trials that began with odor A from trials that began with odor B. The solid white vertical lines denote the 1-second odor 1 presentation. The dotted white vertical line marks the max mean activity of the cell across all trials. The bottom graph is the mean estimated normalized cell activity across all trials. Odor A is in yellow. Odor B is in blue. The red horizontal line is threshold for significant activity.

Figure 2.14.

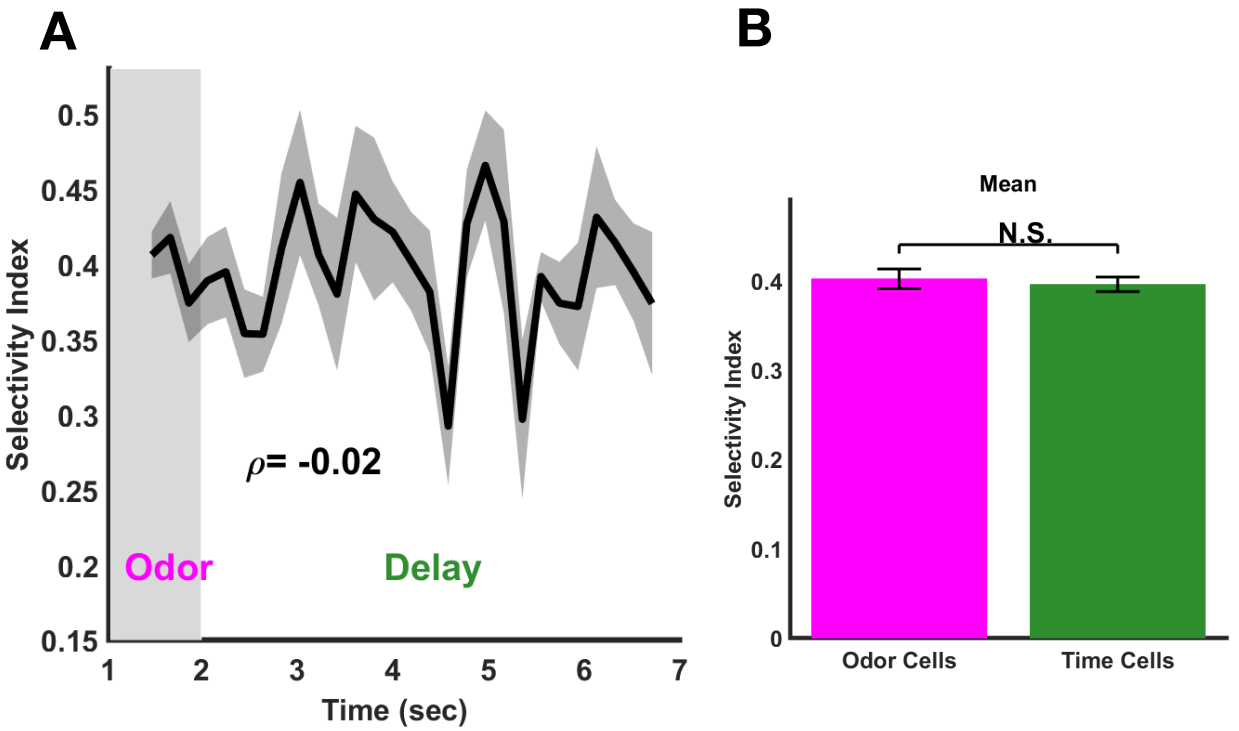

Figure 2.14. CA3 selectivity index is constant across time. (A) Mean CA3 selectivity index across all cells across time (Pearson correlation, ρ = -0.02; p = 0.65) (n = 2443 ± 498.47 cells). Grey shaded region around the line is the standard error. Shaded region from second one to two denotes odor 1 presentation. (B) Comparision of the mean selectivity index between odor and time cells. Mean SI for odor cells was 0.402 ± 0.011. Mean SI for time cells was 0.396 ± 0.008. There was no sigificant difference found between the mean SI for odor and time cells (p = 0.63). Purple denotes odor cells, green denotes time cells.

2.5 DECODING ODOR FROM THE CA3 CELL POPULATION

The low odor selectivity in the CA3 cell population made us wonder if CA3 cells truly held odor or time information. To test this, we tried decoding odor and time from the CA3 cell population.

To decode odor, we used Support Vector Machines (SVM) decoding. SVM decoding is optimal for classifying data between binary classes. Since we are decoding between two odors (odor A and odor B), this SVM decoding is the best choice. We separated sessions into expert sessions, defined as sessions with above 85% accuracy, and novice sessions, defined as session with below 85% accuracy. A SVM decoder was built for each day. The SVM decoder was only trained on correct trials, but was tested on correct and incorrect trials. Using expert sessions, odor was able to be decoded during (1) the odor presentation ($p < 0.05$) and (2) the entire delay period ($p < 0.05$ delay second 1-4) (**Fig. 2.15**). Odor decoding accuracy was highest during odor presentation and dropped as the trial progressed, though staying above the shuffled baseline. Using novice sessions, odor was more accurately decoded during the odor presentation ($p = 0.06$) and the early delay period (**Fig 2.15**). During the latter delay period, accuracy dropped to similar accuracies as the shuffled baseline (**Fig 2.15**). Decoding during expert sessions was significantly better when compared to novice sessions during the majority of the trial ($p<0.05$: odor presentation, delay seconds 1-4).

These findings could be biased because the number of trials used for training the decoder in expert sessions did not match the number of trials used for novice sessions. We accounted for this by subsampling the data. We wanted to create the most stringent measure for subsampling. To do so, we matched the number of correct trials used for training between the expert and novice sessions. We also only used days that had at minimum 66 correct trials for expert and novice sessions. This ensured that the SVM decoder was trained in the same number of trials in expert and novice sessions and that there were sufficient trials being fed into decoder for training. The subsampled SVM decoding resulted in slightly higher accuracy, but the trends in the data were similar to those found in the original SVM decoding results. Using expert sessions, odor was decoded at all time points ($p < 0.5$: odor presentation, delay second 1-4) (Supplementary Fig. 2.4). Using novice sessions, odor was more accurately decoded during the odor presentation and the early delay period ($p < 0.05$: delay second 1) compared to the late delay period. Decoding for novice sessions dropped close to the shuffled baseline during the late delay period (Supplementary Fig. 2.4).

Since odor identity can be decoded from CA3 cells, this population does indeed hold odor information. Odor identity can be decoded at all time points from the first odor presentation to the end of the delay. This implies that mice are retaining information about odor 1 identity in CA3 throughout the delay to compare with odor 2 in order to complete the DNMS task. This is confirmed when comparing SVM odor decoding performance in expert and novice sessions. In expert sessions, mice have learned how to perform the DNMS task correctly.

To do so, mice must retain information on odor 1 identity throughout the delay to compare with odor 2. Only then can mice identify and respond correctly to non-match trials. Therefore, decoding accuracy is high throughout the odor presentation and the delay period. In novice sessions, mice have not yet learned that they must retain information on odor 1 identity to correctly compare it to odor 2.

Figure 2.15.

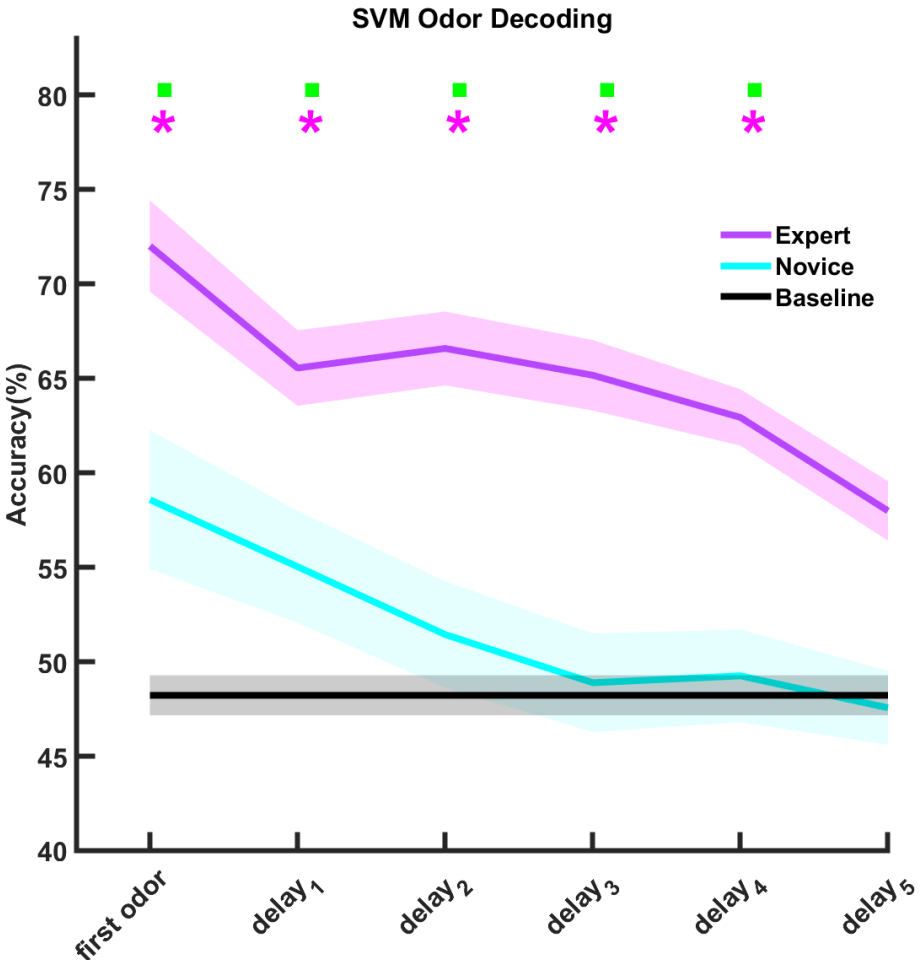

Figure 2.15. CA3 SVM odor decoding across time. Purple line represents mean performance of the SVM decoder during expert sessions. Shaded purple region represents standard error. Cyan line represents the mean performance of the SVM decoder during novice sessions. Shaded cyan region represents standard error. Black line represents the mean performance of the SVM decoder at baseline. Shaded black region represents standard error. Purple asterisks denote $p < 0.05$ for expert sessions compared to baseline. Green squares denote $p < 0.05$ for expert sessions compared to novice sessions. (n = 5 mice)

2.6 DECODING TIME FROM THE CA3 CELL POPULATION

To decode time, we chose to use Bayesian decoding. Bayesian decoding is optimal for continuous data and allows for the incorporation of prior information on the stimulus through a posterior probability. This makes it a good choice when decoding temporal information since time exists on a continuous scale, rather than in distinct classes, and the probability of being at one point in time heavily depends on what the previous point in time was.

A Bayesian decoder was built for each day using the same methods described in the SVM decoding. We measured the accuracy of the Bayesian decoder by comparing the amount of error found to that present in the shuffled baseline.

Using expert sessions, we were able to decode time at levels better than chance during: (1) odor presentation, (2) early delay, (3) late delay ($p < 0.05$) (**Fig. 2.16**). Time decoding was most accurate during the odor presentation and early delay. Using novice sessions, we were able to decode time during: (1) odor presentation and (2) early delay ($p < 0.05$) (**Fig. 2.16**). We were able to decode time more accurately using expert sessions compared to novice sessions during: (1) odor presentation and (2) early delay ($p < 0.05$) (**Fig. 2.16**). Time decoding was the most accurate during the odor presentation and early delay.

Since temporal information can be decoded from CA3 cells, this population does indeed hold temporal information. Using expert sessions, we were able to decode time from the odor presentation, early delay, and late delay.

This is further demonstrated when comparing our results in the well-trained and novice sessions. We see that in novice sessions, time was able to be decoded during the odor presentation and the early delay, but not during the rest of the delay. This signifies the implicit timing of the task is recognized; mice hold timing information on the beginning of the delay. This information decays as the trial goes on and does not improve before the second odor presentation.

While we were able to decode time in the odor presentation and early delay in both well-trained and novice sessions, we were able to decode time significantly better in well-trained sessions ($p<0.05$) (**Fig. 2.16**). CA3 cells held better temporal information during well-trained sessions.

Figure 2.16.

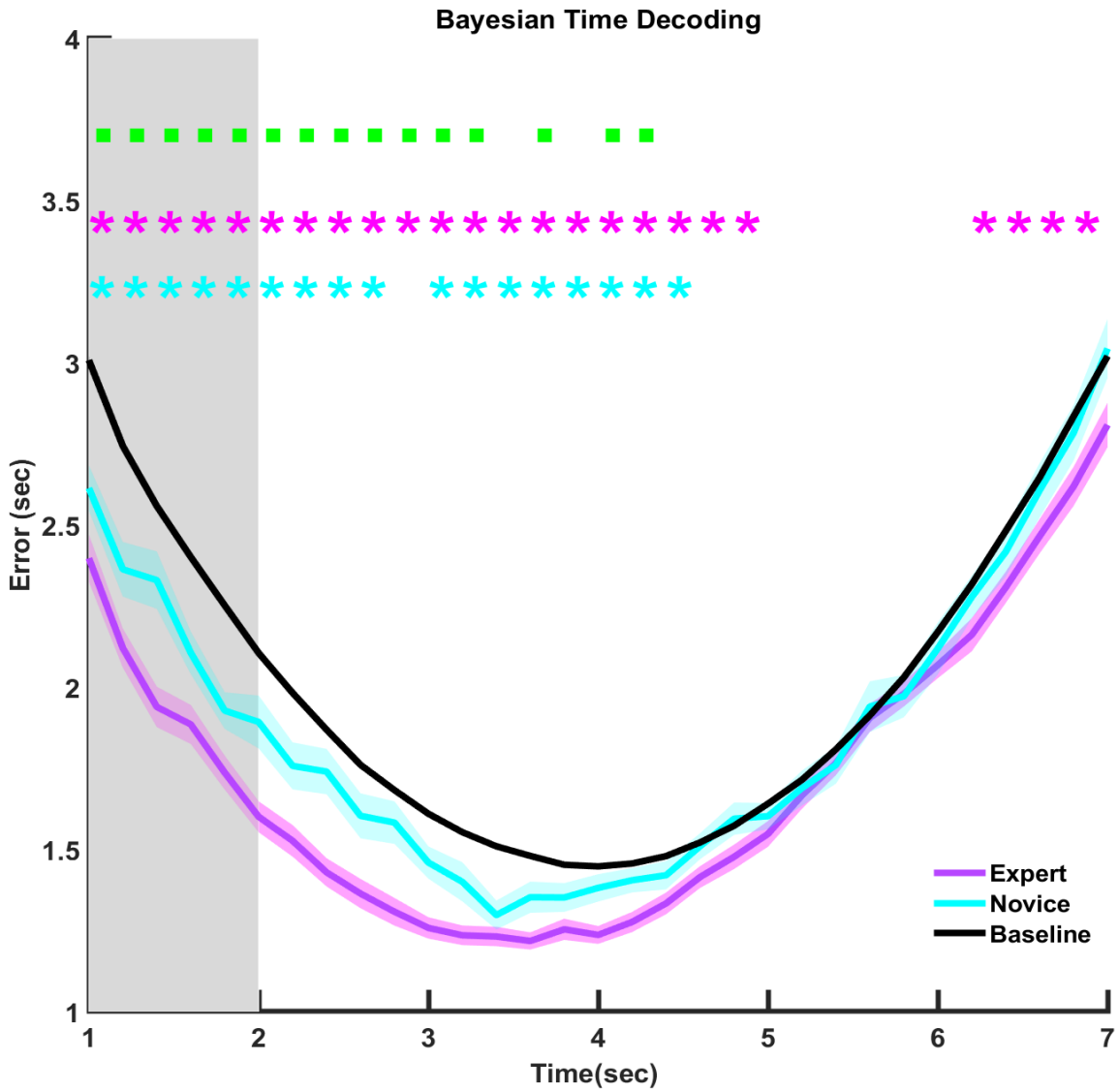

Figure 2.16. CA3 Bayesian time decoding across time. Purple line represents mean performance of the Bayesian decoder during expert sessions. Shaded purple region represents standard error. Cyan line represents the mean performance of the Bayesian decoder during novice sessions. Shaded cyan region represents standard error. Black line represents the mean performance of the Bayesian decoder at baseline. Shaded black region represents standard error. Purple asterisks denote $p<0.05$ for expert sessions compared to shuffled baseline. Cyan asterisks denote $p<0.05$ for expert sessions compared to novice session. Green squares denote $p<0.05$ for expert sessions compared to novice sessions. (n = 5 mice).

2.7 DISCUSSION

In summary, here we report the findings that (1) CA3 cells fire in a sequential manner during a working memory task, (2) CA3 cells process sensory and temporal information, and (3) CA3 cells have low odor selectivity. Our finding of sequential firing in the CA3 cell population is novel as CA3 has never been imaged during an olfactory modified working memory task. This finding helps shed light on the role that CA3 cells play in non-spatial memory. We found that CA3 cells encode odor and time information in odor cells and odor-specific time cells. We also found that time and odor information can be decoded from CA3 cells. This proves that CA3 cells do indeed process sensory and temporal information. Finally, we found that CA3 cells interestingly have low odor selectivity. This is despite being able to accurately decode specific odor information from population.

These findings together indicated a small subpopulation of CA3 cells held enough information to drive decoding. The remaining majority were low odor selectivity cells. The SI index distribution supported this conclusion. While the mean SI index for all cell groups was low, there were cells that had high SI and were very selective for a particular odor. When a cell population is fed into the decoder, the decoder does not weigh each cell equally. If certain cells help the decoder guess the correct answer better, those cells are weighted more. This explains why we were able to decode odor accurately from a population of mostly low odor selectivity cells.

How does CA3 compare to CA1? Our findings were that (1) CA3 has similar sequential firing patterns as those found in CA1, (2) CA3 processes sensory and temporal information and CA1 was found to as well, (3) CA3 has lower selectivity than CA1 cells.

We were able to compare grossly the sequential firing patterns in CA1 and CA3. Both cells that fire during the odor presentation and cells that tile the delay. This is also consistent with the literature on CA1 and CA3 within the field, as discussed in Chapter 1.

Both CA1 and CA3 process sensory and temporal information. While we found fewer percentage of odor cells and odor-specific time cells in CA3 as compared to those found in CA1, this is due to the difference in stringency in the defining of these groups. We only categorized cells as odor cells or odor-specific time cells if their activity was above the 99th percentile of the shuffled activity distribution. Taxidis et al. used a threshold the 95th percentile of the shuffled activity distribution. Given this, it makes sense that we would identify fewer odor cells and odor-specific time cells. Due to anatomy, we also were not able to image the same number of CA3 cells as can be imaged in CA1. When imaging CA1, the objective lens is parallel to the surface of CA1. Thus, the CA1 cells populate the entire field of view. Whereas for CA3, the objective is parallel to the curve of CA3. This means the field of view is constrained to a strip of cells, since the objective is viewing sections of the CA3 curve. The sheer number of cells that are possible to image in a single field of view is lower for CA3 compared to CA1.

Using CA3 cell activity, we were able to decode odor during odor presentation and the following time delay during both expert and novice sessions. During the odor presentation, the mouse is acutely experiencing the odor, so the odor identity is known. This is why odor is still able to be decoded during the odor presentation in novice sessions. As the mouse enters the delay period, and the experience of the odor becomes further in the past, the mouse "forgets" the odor identity. This is why the SVM decoding accuracy, which reflects the information held in the CA3 cell population, drops during the delay in novice sessions. This phenomenon is seen in expert sessions as well, but the overall accuracy of the SVM odor decoding is higher in expert sessions compared to novice sessions. Mice in expert sessions had learned the salience of the odor, and therefore learned to store more information regarding odor identity.

Using CA3 cell activity, we were able to decode time during the odor presentation, early delay, and late delay in expert sessions. This is in line with the timing demands of the DNMS task. The task itself does not require explicit timing. That is, the task does not require mice to attend to the temporal dimension of the task by responding to a specific time interval. The DNMS task does include implicit timing. Though there was no explicit instruction to process time, timing was still inherent in the set five second delay between odor presentations. This timing affected behavior and cognition. Well-trained mice may not count each second during the delay, but may perceive that following the first odor presentation there will be a delay of some length and that, towards the end of the day, a second odor will be presented. This was evident when examining the lick patterns in mice as they learn the DNMS task. During

the lick shaping step of DNMS training, untrained mice start off by licking through the entire trial. Because they have not learned the temporal structure of the DNMS task yet, they do not know to withhold their licking to the response window following odor two presentation. Towards the end of the lick shaping step, mice have learned the temporal structure of the DNMS task. They no longer lick throughout the trial. Instead, they withhold their licking to the response window. This demonstrated understanding of the temporal structure of the DNMS task and that mice were utilizing some temporal processing while performing the task.

Our results in expert and novice sessions reflected this understanding of the temporal structure of DNMS. Mice in expert sessions were more attuned to timing at the beginning of the delay because they recognized that a delay was beginning. Timing was less important in the middle of the delay, as that information was not needed for behavior, anticipation, or decisions. Towards the end of the delay, timing became salient again as the mouse anticipated the presentation of the second odor. Thus, time can be decoded during the odor presentation, early delay, and late delay, but not during the middle (delay second 3-4) delay in expert sessions. Mice in novice sessions do not fully understanding the importance of the second odor and therefore not being attuned to its timing. The second odor is not salient to them because they have not learned that it is tied to a possible reward. Thus, time cannot be decoded from the late delay in novice sessions. Overall, the SVM odor decoding was higher in expert sessions compared to novice sessions. This shows that while the temporal structure of the DNMS task was learned in both expert and novice sessions, temporal

information was more salient in expert sessions. During expert sessions, the mice were more attuned to the timing of the task. Perhaps this temporal information held in the CA3 cells helped them to accurately anticipate and respond more accurately than in novice sessions.

In comparing CA1 and CA3 decoding, we found that while CA1 and CA3 can both decode odor, CA3 was better at decoding time than CA1. In CA1, decoding of temporal information was found to decay significantly towards the end of the delay during the DNMS task (Taxidis et al., 2020). Using CA3 cells, time was decoded from the late delay of the DNMS task. This implies that CA3 holds and processes more temporal information than CA1 does. It is unclear how comparable time decoding in CA1 is to CA3 though, as the shape of the shuffled baseline in the CA1 study differs from our CA3 study. This could indicate a difference in methodology used to obtain the shuffled baseline, differences in the calcium analysis pipeline, or an inherent difference in how temporal information is processed in CA1. Regardless, these results could point to CA3 being the region temporal information is processed, as more temporal information regarding the DNMS task seems to be processed there. Since the DNMS task only has implicit timing, CA3 could process the task temporal information and then only pass the portion deemed relevant to CA1.

Finally, we found that CA3 cells have lower odor selectivity than CA1 cells. CA3 cells on average have a lower odor SI than CA1 cells. This is interesting because it speaks to the differences in the role of CA3 and CA. CA1 is the output of the hippocampus and does not necessarily have to produce its own code. This could mean that it does not need the flexibility

of a large population of low selective cells, since it is mainly reading information from inputs. CA3 has a large population of non-selective cells that have the flexibility to hold multimodal information. If CA3 is indeed integrating sensory and temporal information, it requires this population of cells that can easily adapt and learn fast in order to quickly produce a stable rule that can be passed on.

2.8 METHODS

CA3 Viral Injection and Cranial Window Implantation Surgery

Adult (10-15 week old) male or female Girk4-cre mice were anesthetized with 5% isoflurane to induct and then given 1.3-1.5% isoflurane to maintain general anesthesia. Prior to surgery, lack of eye blink and withdrawal to foot pinch reflexes were confirmed to ensure that animals were under the effect of the general anesthesia. Ophthalmic ointment was applied to the animal's eyes to prevent drying and discomfort during the surgery. The animal was placed in a stereotaxic frame and body temperature was controlled using a Harvard Apparatus body temperature regulator and heating pad. The fur on the skull was shaved with an electric razor followed by a chemical depilatory (Nair). The animal was prepped and draped in a sterile manner. Carprofen (an analgesic), dexamethasone (an anti-inflammatory drug), and saline, to replace fluids lost during surgery, were injected subcutaneously. The scalp was infiltrated with lidocaine, a local analgesic. The scalp was sanitized with betadine and 70% ethyl alcohol. The scalp and underlying tissue were incised with a scalpel blade. The skull was scraped using the scalpel blade to facilitate effective bonding between the skull and head-bar. A small (3 mm diameter) craniotomy was made on the right hemisphere above CA3 using an air-powered precision dental drill, with great care taken to not disrupt the dural sinuses. The site was flushed with chilled cortex buffer until bleeding subsided. Mice then received a 500nL viral injection of a 1:10 dilution of filtered phosphate buffer solution (PBS) and AAV1-syn-FLEX-jGCaMP7f-WPE (10^{12} viral particle dilution) at a rate of 1 nL/second into CA3. Nanoject viral injectors and Zeiss STEMI-100 surgical scopes were used. After viral injection is complete, the glass needle was left in brain for 30 minutes to allow for viral

spread. The glass needle was then slowly removed from the injection site. Cortex above the hippocampus was removed through vacuum suction. A cannula with 3mm diameter, 1.5 mm height, and a #1-thickness cover-glass window was implanted in the craniotomy above CA3. The cannula was bonded to the skull with a thin layer of VetBond tissue adhesive followed by a layer of cyanoacrylate glue. A customized omega-shaped head-bar was fixed on the skull using dental cement. The dental cement layer covered the exposed skull and bonded to the cannula. The cannula was filled with Kwik-Sil to protect against debris and dust entering the cannula. Animals were provided amoxicillin, an antibiotic, treated water over 14 days.

Two-photon calcium imaging of CA3

Animals recovered for 14 days after surgery and then were water-deprived to 85%-90% their initial body weight. They then were acclimated to head-restraint and imaged while learning or stably performing the olfactory modified delayed-non-match-to-sample (DNMS) task. Animals were trained every day and received all their daily water requirements as they performed the task. If mice do not drink 1 mL of water during the task, their water dose was supplemented after task performance. Animals were weighed every day to ensure that body weight did not drop below 85% of original body weight. All behavioral training and testing were done in high throughput, automated animal behavioral setups.

The animals were imaged using a Scientifica microscope that uses a high-power Ti-Sapphire Coherent Ultra 2 laser. This laser had a max power at 800nm 3.7 Watts, which is sufficient

for powering two separate two-photon microscopes. The laser was routed to a Sutter MOM *in vivo* two-photon microscope equipped with 2 PMTs (Hamamatsu) and galvanometric mirrors (CambridgeTech) for fast scanning, and 5X,16X, 20X, and 40X Olympus objectives for imaging, and a rotatable objective head that allowed for varied imaging angles, perpendicular to the brain surface. It was also routed to a Scientifica resonant scanning microscope (32 Hz full frame imaging, 2 channels), equipped with a Gallium-Arsenide PMTS, and filters for green and red channel imaging. Proprietary Scientifica software drove acquisition through high-rate data acquisition devices. A custom Scientifica computer was equipped with the appropriate NIDAQ cards for digitizing the PMT signal after amplification through Stanford preamplifiers. An *in vivo* rig was attached to the microscope for head-fixed behavioral assays. The chamber was built identical to those described in the "Behavioral Training" section, but in addition were equipped with custom-made motion detectors for quantification of the spherical treadmill velocity and direction. Blood vessel patterns and precise alignment of the animal were utilized to image the same set of neurons each day. We recorded at 920 nm, 30 Hz, 512 x 512 pixel frames, and an average power of 118.5 mW. This gave us a field of view of 500x500 μm.

Behavioral Training – Olfactory Modified Delayed Non-Match-to-Sample Task

Mice were presented with two odors with a five second delay between presentations. Mice were taught to lick when the odors are not the same. Mice must remember the first odor, hold the memory for five seconds, and compare it to the second odor to give the correct response. Following surgery, mice were gradually habituated to the behavioral set-up. The

lick-shaping stage consisted of only non-match trials to encourage mice to lick following the second odor. In first few days of the lick-shaping stage, a water droplet was presented to the mouse through the lickport after odor 2 presentation, regardless if the mouse licked in the response window or not. This taught the mouse to receive water through the lickport following odor 2. In the latter days of the lick-shaping stage, the mouse must lick the lickport following odor 2 for a water droplet to be dispensed. This taught the mouse they must lick the lickport after odor 2 to receive water. By day 14, matched trials were introduced, and mice learned to differentiate between matched and nonmatched trials. Mice underwent 8-12 sessions of 20 trials each per day. By day 20, mice were generally well-trained and performed consistently above 80%.

The mice were trained in two self-contained behavioral rigs. Each setup included the following components: (1) a ventilated sound-proof box containing a spherical treadmill, (2) custom posts and headbars to head-fix animals onto the spherical treadmill, (3) Island Motion Lick detection equipment for measuring licking of water from the lick-tube, (4) infra-red camera for recording mouse behavior, and (5) silent fans for ventilation. A multichannel olfactometer outside of the box delivered odors to each of the boxes through connecting tubes. Each olfactometer served two behavioral boxes. A computer running custom software in MATLAB using NIDAQ digital/analog devices controlled reward delivery and kept track of mouse performance. Another setup that included a motion detector to track the velocity and direction of the spherical treadmill was integrated with the two-photon set-up.

Quantification and Statistical Analysis

Analysis of Calcium Imaging Data

Preprocessing: Preprocessing of image data was carried out with custom scripts written in MATLAB (Mathworks, Natick, MA, USA) and the calcium imaging analysis package, Suite 2P (Pachitariu et al., 2017). To denoise the signal, the raw image data was first passed through a 3Hz low-pass filter using a custom MATLAB script. Then, the signal was deconvolved using the deconvolution script from Suite2P (Friedrich et al., 2017; Patchitariu et al., 2018). The image was then put through the entire Suite2P package for motion correction and ROI extraction. Following this, the signal was normalized per trial according to the max signal, based on the 6 second time period beginning at the presentation of odor 1 to the end of the 5 second delay (Supplementary Fig. 2.1). A baseline was created based on the mean activity during the one second before presentation of odor 1. A threshold of two standard deviations above this baseline was set. Signal that fell below this threshold was set to 0 (Supplementary Fig. 2.1).

Defining Significant Cells:

Mean activity over all trials was computed for each cell. The time-bin in which the maximum average activity occurs was considered the firing field of that cell. The cell activity trace for each trial was then flipped and circularly shifted by a random interval in either the positive or negative direction. Maximum mean cell activity over the shifted trials was computed. This was repeated 500 times to generate a baseline distribution of maximal mean cell activity. If a cell had a maximum average estimated cell activity larger than the 99th percentile of the

shuffled distribution, it was considered to have a significant field. An odor cell was defined as having a significant firing field in the time-bin of the odor presentation. Cells that had significant firing fields in the delay period following the first odor presentation were considered time cells.

Odd vs. Even validation:

Odd trials during the sequence cells' preferred odor trials were sorted by the time-bin of each cell's maximal mean activity. This created the sequential activity that was seen when all trials were sorted together. We then took then took the index of these cells and sorted the even trials by this order.

We compared the correlation of even and odd trials to a shuffled baseline. We calculated the correlation between each row of the even trials to the corresponding row of the odd trials. We created a shuffled baseline by flipping and circularly shifting the cell activity for each trial by a random interval in either the positive or negative direction. We then calculated the correlation between even and odd trials in the shuffled data in the same manner as in the original data. The two distributions were compared through a Wilcoxon rank-sum test.

Odor Selectivity Index:

Odor selectivity index was calculated as the ratio of $(R_{pref} - R_{nonpref})/(R_{pref} + R_{nonpref})$. Each cell's activity was averaged across all trials. R_{pref} is the estimated activity at the single time-bin of

the cell's maximal mean activity during preferred odor trials. $R_{nonpref}$ is the estimated mean activity at that same time-bin, but in the non-preferred odor trials.

Odor SI across time correlation was calculated through a Pearson's correlation.

SVM odor decoding:

SVM decoding was carried out through custom scripts written in Python (Rossum, 1995). We have a cohort of 5 mice. There were 50 days of experimentation total across all mice. During each day, there were 8 - 13 sessions. Each session consisted of 20 trials of the DNMS task. Analysis was limited to the time period from the beginning of odor 1 presentation to the end of the five second delay. We separated sessions into either expert or novice sessions. Expert sessions were defined as sessions with above 85% accuracy (at minimum 17/20 trials correct). Novice sessions were defined as sessions with below 85% accuracy. We then took either the expert sessions or novice sessions and concatenated all the trials from the sessions into one matrix. We labeled the correct and incorrect trials in this matrix. Then, 80% of the trials were randomly selected. Out of this selection, only the correct trials were used to train the decoder. If there were less than 20 correct trials in this selection, the session was excluded due to insufficient data. The remaining 20% of the data was using for testing. Both incorrect and correct trials were used for training. The baseline was created using the data from the one second before odor 1 presentation. This data was run through the SVM decoder in the same way as stated above. The result was the concatenated across

all time-bins to create a baseline. Significance was determined through a Wilcoxon rank-sum test.

SVM odor decoding, subsampling:

The number of correct trials used for SVM decoder training were matched between expert and novice sessions. Only days with a minimum of 66 correct trials for expert and novice sessions were used. The rest of the SVM decoding was performed as in the non-subsampled SVM decoding.

Bayesian time decoding:

Bayesian decoding was carried out through custom scripts written in Matlab (Mathworks, Natick, MA, USA). We have a cohort of 5 mice. There were 50 days of experimentation total across all mice. During each day, there were 8-13 sessions. Each session consisted of 20 trials of the DNMS task. Analysis was limited to the time period from the beginning of odor 1 presentation to the end of the five second delay. We used 31 time bins across the seven seconds included in the analysis (0.23 seconds per time bin). We parsed the sessions into expert and novice sessions using the same definition and methods as described in the SVM odor decoding methods. We trained and tested the Bayesian decoder using the same methods as described in the SVM odor decoding methods. The error in seconds was graphed. Significance was determined through a Wilcoxon rank-sum test.

The shuffled baseline was created using the data from the well-trained sessions, as this would create a more stringent baseline than if the novice sessions were used. Each trial was flipped then and circularly shifted by a random interval in either the positive or negative direction. The data was then run through the Bayesian decoder in the same way as stated above. The error in seconds was graphed to represent the shuffled baseline.

Confocal Images

Images were obtained using a Zeiss LSM 800 confocal microscope or Zeiss apotome 2. Fiji (Image J) was used for figure preparation.

2.9 SUPPLEMENTARY FIGURES

Supplementary Figure 2.1.

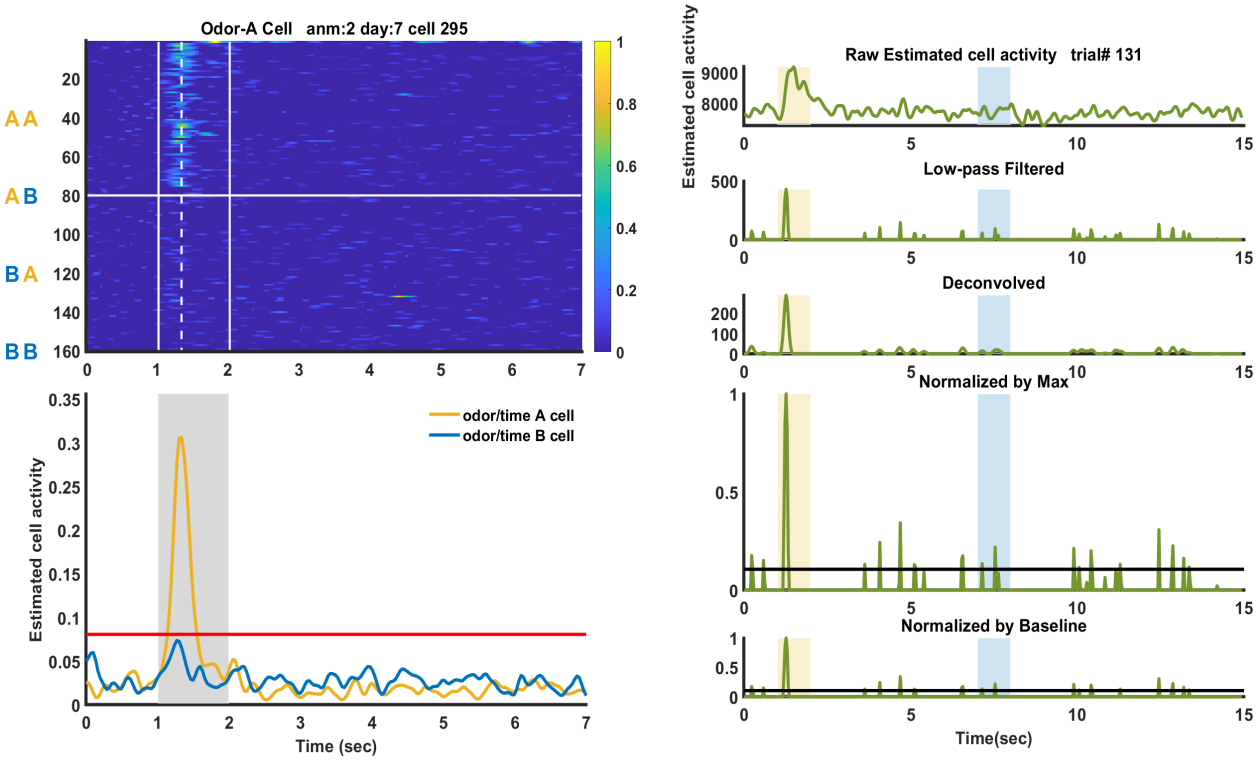

Supplementary Figure 2.1. Example of pre-processing steps. Left: The top graph is a heatmap of the normalized estimated activity of one cell across 160 trials. Each row is one trial. The trials are split up into the four possible odor presentation combinations (AA, AB, BA, BB). The solid white horizontal line separate trials that began with odor A from trials that began with odor B. The solid white vertical lines denote the 1-second odor 1 presentation. The dotted white vertical line marks the max mean activity of the cell across all trials. The bottom graph is the mean estimated normalized cell activity across all trials. Odor A is in yellow. Odor B is in blue. The red horizontal line is threshold for significant activity. Right: Graphs in order from top to bottom, according to the flow of pre-processing steps. Black line indicates baseline, as calculated from the activity one second before odor 1 presentation. See methods for detailed description.

Supplementary Figure 2.2.

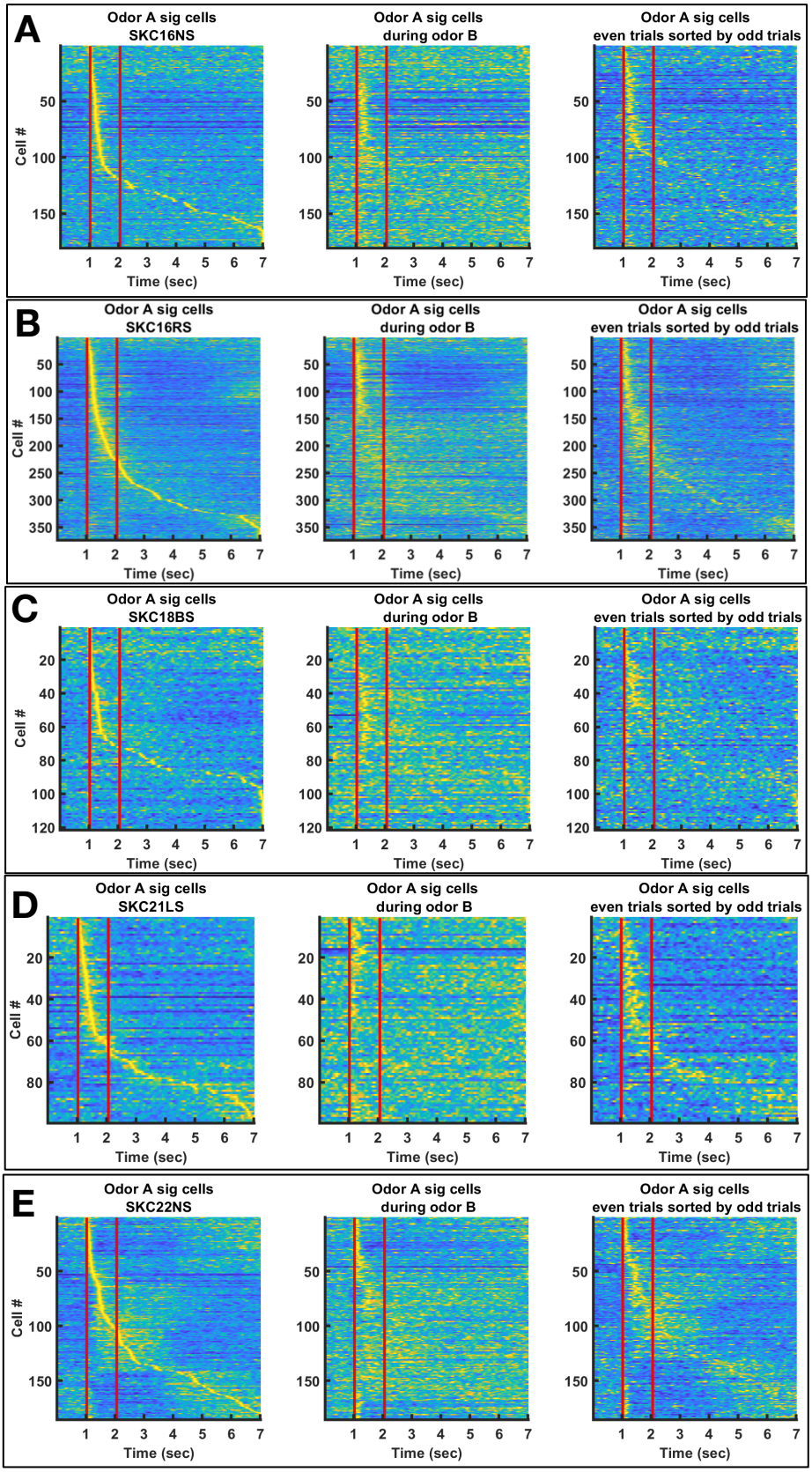

Supplementary Figure 2.2. CA3 Odor A cells sequential activity, mouse variability. (A)-(E) CA3 Odor A cells sequential activity in odor A trials (left graph), odor B trials (middle trials), and in odor A even trials sorted by odor A odd trials (right graph). Each set of three graphs represents data from one mouse (SKC16NS, SKC16RS, SKC18BS, SKC21LS, SKC22NS) (n = 5 mice). Red vertical lines denote the time-bin of odor presentation.

Supplementary Figure 2.3.

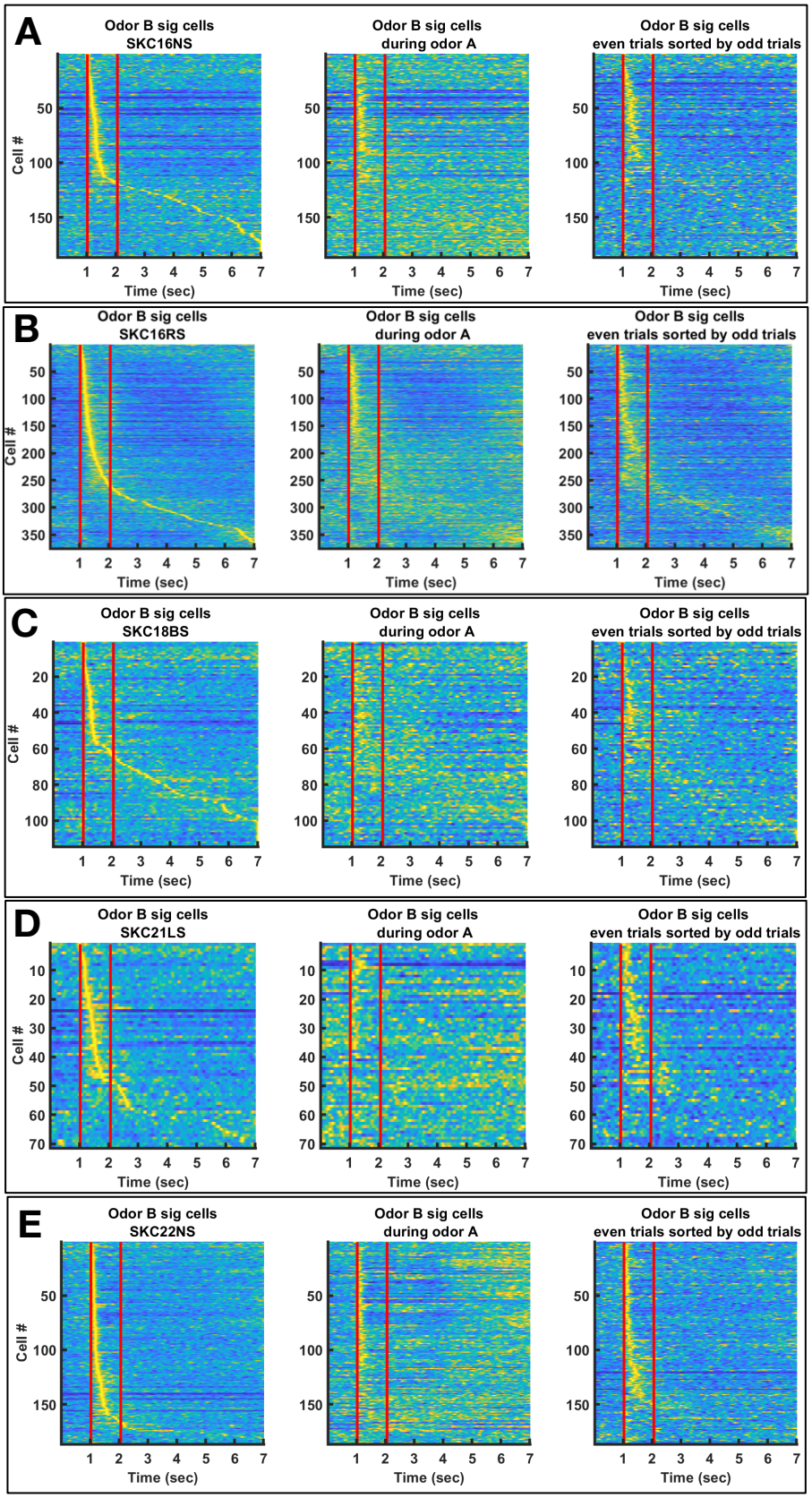

Supplementary Figure 2.3. CA3 Odor B cell sequential activity, mouse variability. (A)-(E) CA3 Odor B cells sequential activity in odor B trials (left graph), odor A trials (middle trials), and in odor B even trials sorted by odor B odd trials (right graph). Each set of three graphs represents data from one mouse (SKC16NS, SKC16RS, SKC18BS, SKC21LS, SKC22NS) (n = 5 mice). Red vertical lines denote the time-bin of odor presentation.

Supplementary Figure 2.4.

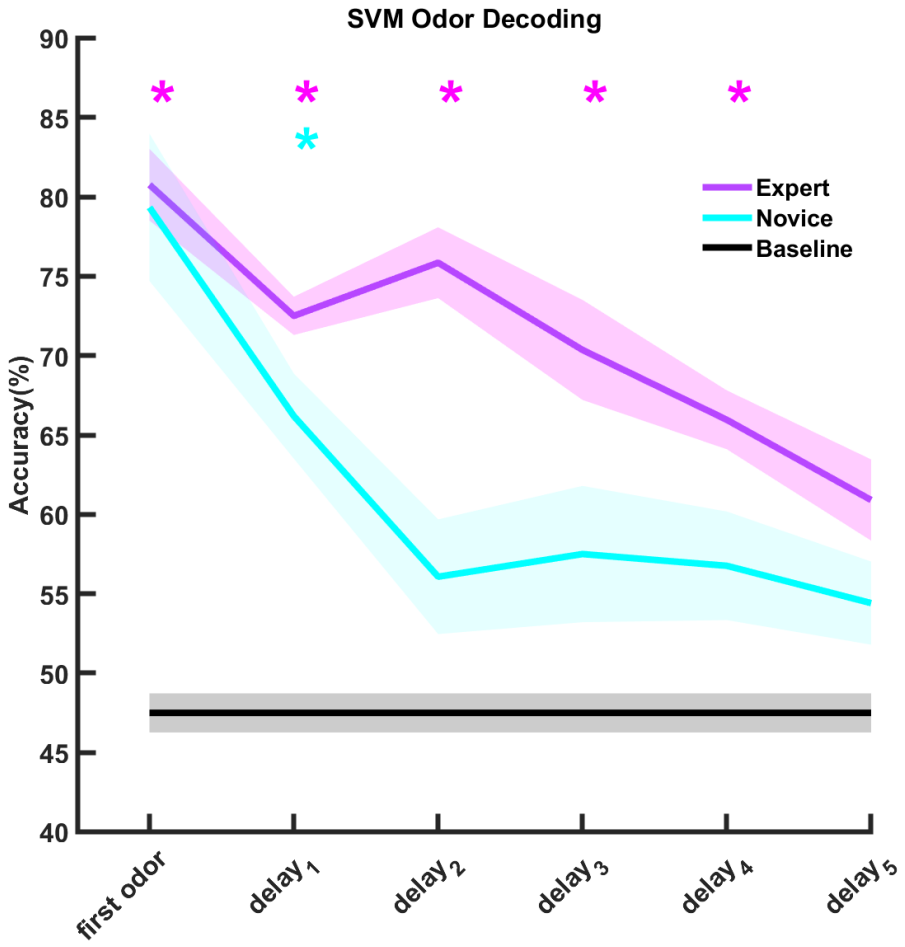

Supplementary Figure 2.4. SVM odor decoding across time, data subsampled. Purple line represents mean performance of the SVM decoder during expert sessions. Shaded purple region represents standard error. Cyan line represents the mean performance of the SVM decoder during novice sessions. Shaded cyan region represents standard error. Black line represents the mean performance of the SVM decoder at baseline. Shaded black region represents standard error. Purple asterisks denote $p < 0.05$ for expert sessions compared to baseline. Cyan asterisks denote $p < 0.05$ for expert sessions compared to novice sessions. (n = 5 mice)

2.10 REFERENCES

Friedrich, J., Zhou, P., & Paninski, L. (2017). Fast online deconvolution of Calcium Imaging Data. PLOS Computational Biology, 13(3). https://doi.org/10.1371/journal.pcbi.1005423

Liu D, Gu X, Zhu J, Zhang X, Han Z, Yan W, Cheng Q, Hao J, Fan H, Hou R, Chen Z, Chen Y,
Li CT. Medial prefrontal activity during delay period contributes to learning of a working memory task. Science. 2014 Oct 24;346(6208):458-63. doi: 10.1126/science.1256573. PMID: 25342800.

Nakazawa K, Quirk MC, Chitwood RA, Watanabe M, Yeckel MF, Sun LD, Kato A, Carr CA, Johnston D, Wilson MA, Tonegawa S. Requirement for hippocampal CA3 NMDA receptors in associative memory recall. Science. 2002 Jul 12;297(5579):211-8. doi: 10.1126/science.1071795. Epub 2002 May 30. PMID: 12040087; PMCID: PMC2877140.

Pachitariu, M., Stringer, C., & Harris, K. D. (2018). Robustness of spike deconvolution for neuronal calcium imaging. The Journal of Neuroscience, 38(37), 7976–7985. https://doi.org/10.1523/jneurosci.3339-17.2018

Pachitariu, M., Stringer, C., Dipoppa, M., Schröder, S., Rossi, L. F., Dalgleish, H., Carandini, M., & Harris, K. D. (2016). Suite2p: Beyond 10,000 neurons with standard two-photon microscopy.

Taxidis J, Pnevmatikakis EA, Dorian CC, Mylavarapu AL, Arora JS, Samadian KD, Hoffberg EA, Golshani P. Differential Emergence and Stability of Sensory and Temporal Representations in Context-Specific Hippocampal Sequences. Neuron. 2020 Dec 9;108(5):984-998.e9. doi: 10.1016/j.neuron.2020.08.028. Epub 2020 Sep 18. PMID: 32949502; PMCID: PMC7736335.

van Rossum, G. (1995). Python reference manual. Department of Computer Science [CS]. CWI.

Zhang X, Yan W, Wang W, Fan H, Hou R, Chen Y, Chen Z, Ge C, Duan S, Compte A, Li CT. Active information maintenance in working memory by a sensory cortex. Elife. 2019 Jun 24;8:e43191. doi: 10.7554/eLife.43191. PMID: 31232695; PMCID: PMC6634975.

Chapter 3

CA3 stability

3.1 INTRODUCTION

Both CA1 and CA3 process temporal and sensory information. But where does the temporal signal originate? While CA1 odor cells are reliably activated across DNMS trials and retain stable fields over days and extended delays, CA1 odor-specific time cells have unreliable activation and unstable fields over days, with different groups of neurons representing time elapsed after each odor after each day. In addition, the number of CA1 odor-specific time cells increases over days of learning and performing the DNMS task (Taxidis et al., 2020). These characteristics indicate dynamic temporal encoding that remaps day-to-day. However, a stable code would be advantageous for maintaining and reliably re-accessing a memory. CA3 has a recurrent network that can quickly create and store such a code (Rolls, 2013). As an attractor network, CA3 may be able to form quick and strong associations between stimuli and time and re-activation of these associations can occur easily.

Here, I will investigate the stability of the CA3 cells during the DNMS task and compare the results with those found in CA1. We expect to find that CA3 cells are more stable than CA1 cells. We hypothesize that CA3 provides a stable, easily re-accessible association of odor and time that can be passed onto CA1.

3.2 CA3 RELIABILITY

We began to investigate CA3 stability by first looking at the reliability of CA3 cells. We measured reliability by how often a cell fired during its firing field. We found the time point at which a cell had its maximum mean activity across all preferred odor trials in one day. We set narrow bounds for a cell firing field around this time point. Then, we counted the number of individual preferred odor trials in which the cell had activity during in the cell firing field. We divided this number by the total number of preferred odor trials to calculate the cell reliability.

CA3 cell reliability dropped during odor 1 presentation, then was fairly stable over time (Pearson correlation for delay, $\rho = 0.01$; $p = 0.65$) (**Fig. 3.1A**). The mean odor cell reliability was 37.81% ± 0.38. The mean time cell reliability was 29.67% ± 0.26 (**Fig. 3.1B**). There was a significant difference between the mean reliabilities of odor cells and odor-specific time cells ($p = 2.09 \times 10^{-53}$) (**Fig. 3.1B**).

Reliability was calculated in a similar way for CA1 in Taxidis et al 2020. In CA1, reliability, or activation probability, began around 30% at the first odor presentation and dropped to close to 10% by the end of the trial.

Figure 3.1.

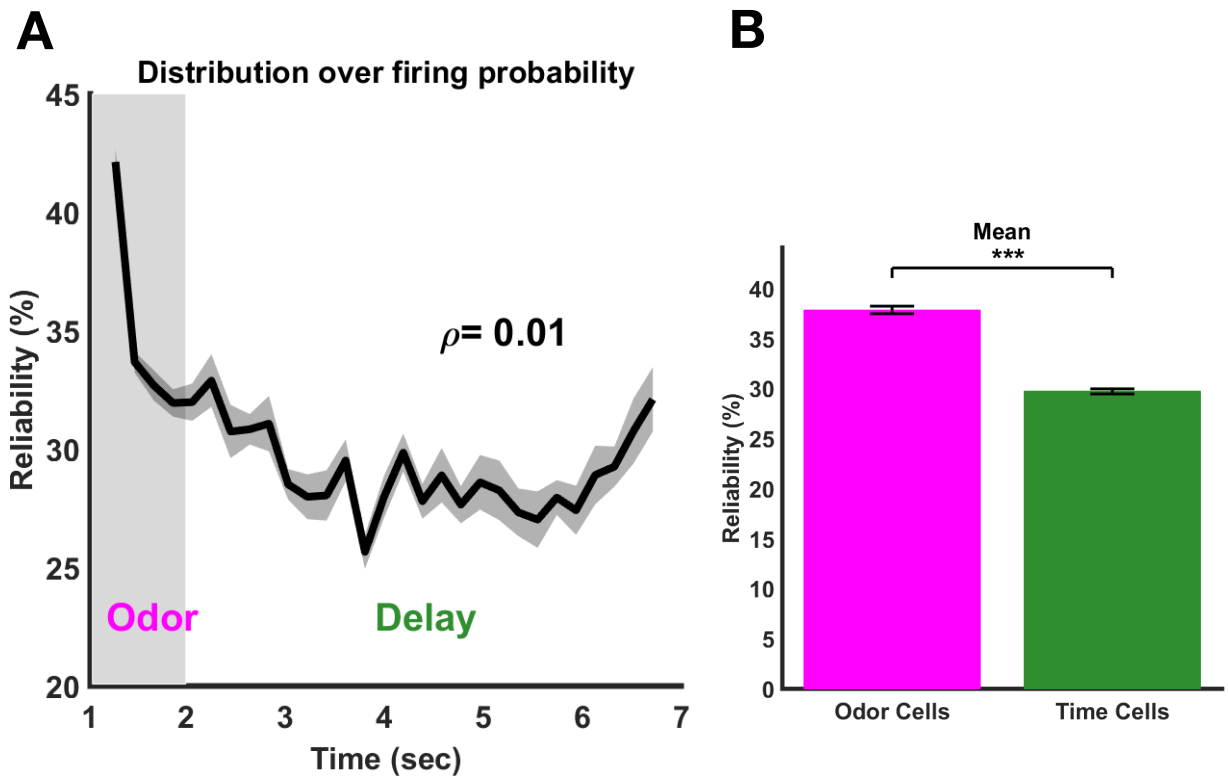

Figure 3.1. CA3 cell reliability. (A) Mean cell reliability across time (Pearson correlation, ρ = 0.01; p = 0.65). All cells pooled across all mice (n = 2443 ± 498.47 cells). Grey shaded region around the line is the standard error. Shaded region from second one to two denotes odor 1 presentation. (B) Comparision of the mean cell reliability (cell firing probability) between odor (37.81% ± 0.38) and time cells (29.67% ± 0.26). There was a significant difference ($p = 2.09 \times 10^{-53}$). ***$p < 0.001$

3.3 CA3 ODOR CELL NUMBERS DO NOT INCREASE ACROSS DAYS

We wanted to look at another measure of stability, so we determined if the number of odor cells or odor-specific time cells increased across days. If the number of odor or odor-specific time cells increased, it could mean that the neural representation of odor or time is changing as the mouse learns and solidifies the memory of the DNMS task. The mouse could be integrating more olfactory or temporal information that is relevant to the task. If the number of odor or odor-specific time cells do not increase, it could mean that the mouse has already created a stable representation of odor and time in the DNMS task.

We calculated the percent of odor cells out of all identified cells. This percentage was calculated for each animal on each day of the DNMS task. Since total cell numbers varied across mice and across days, we chose to use a percentage instead of the raw number of cells so that we could accurately combine the data from each mouse. Overall, we found that the odor cells numbers do not increase across days (Pearson correlation, $\rho = 0.11$; $p = 0.24$) (Fig. 3.2). This held true even when breaking the odor cells into odor A cells (Pearson correlation, $\rho = 0.16$; $p = 0.31$) and odor B cells (Pearson correlation, $\rho = 0.19$; $p = 0.24$) (Supplementary Fig. 3.1).

Figure 3.2.

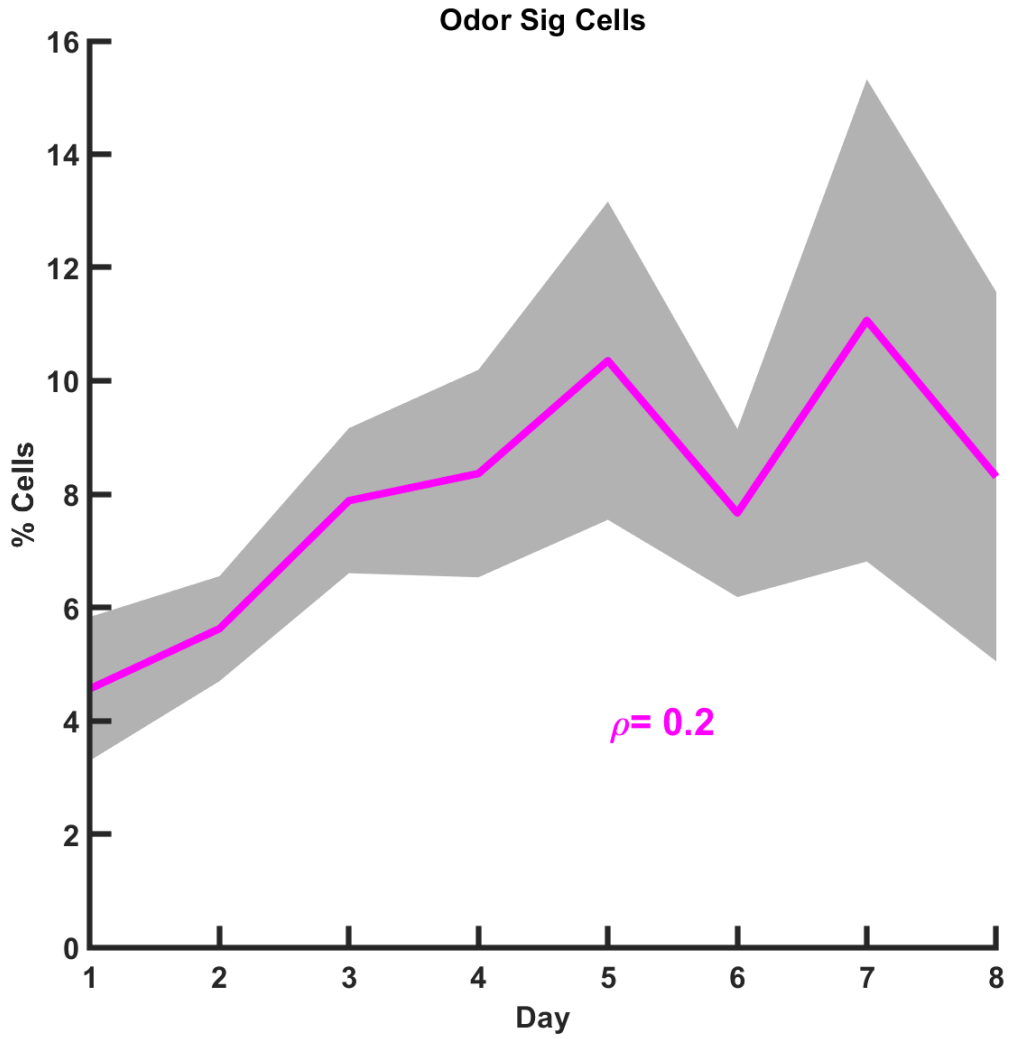

Figure 3.2. CA3 odor cells numbers do not increase across days. (A) Mean percent of odor cells across days (Pearson correlation, $\rho = 0.11$; $p = 0.24$). Cells pooled per animal ($n = 5$ mice). Shaded grey region denotes the variance across animals.

3.4 CA3 ODOR-SPECIFIC TIME CELL NUMBERS DO NOT INCREASE ACROSS DAYS

We next looked to see if the odor-specific time cell population increased across days. We calculated the percent of odor-specific time cells out of all identified cells. This percentage was calculated for each animal on each day of the DNMS task. Since total cell numbers varied across mice and across days, we chose to use a percentage instead of the raw number of cells so that we could accurately combine the data from each mouse. Overall, we found that the odor-specific time cells numbers do not increase across days (Pearson correlation, $\rho = -0.08$; $p = 0.96$) (**Fig. 3.3**). This held true even when breaking the odor-specific time cells into odor-specific time A cells (Pearson correlation, $\rho = 0.08$; $p = 0.61$). and odor-specific time B cells (Pearson correlation, $\rho = 0.01$; $p = 0.94$). (**Supplementary Fig. 3.2**).

Figure 3.3.

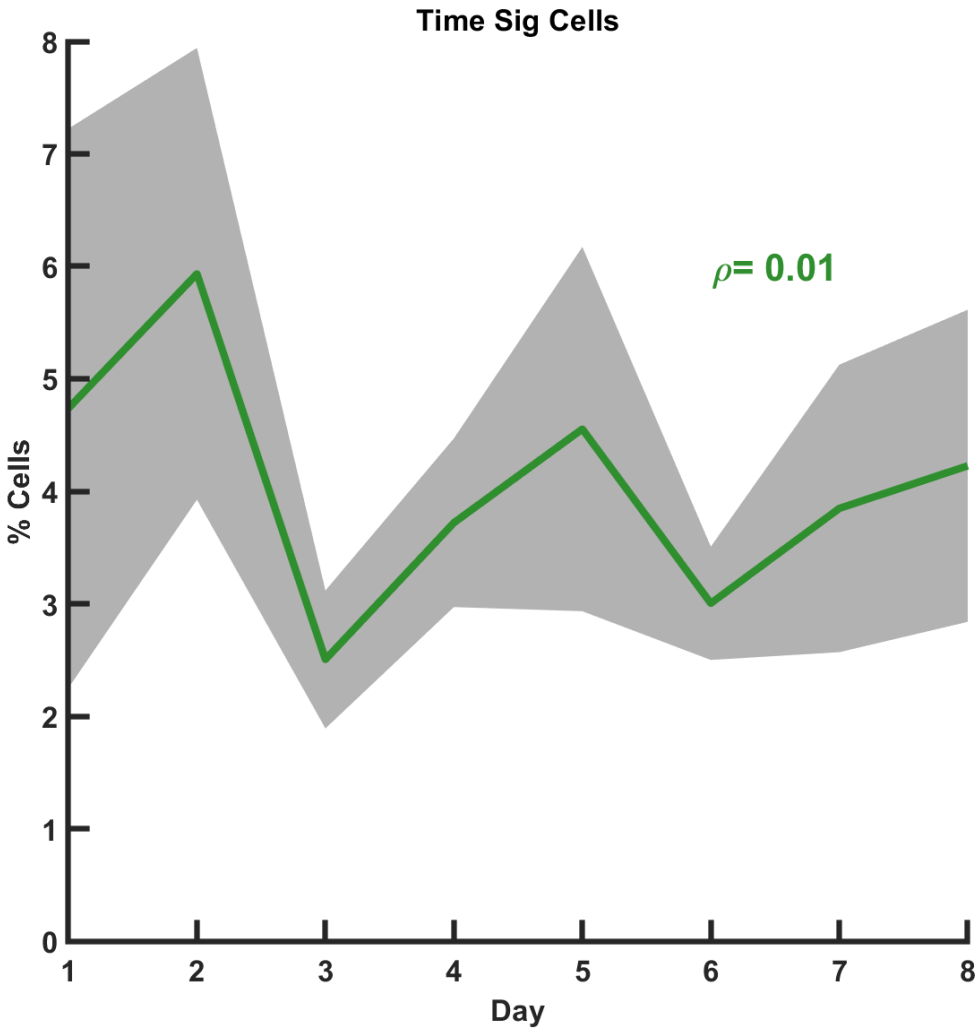

Figure 3.3. CA3 odor-specific time cells numbers do not increase across days. Mean percent of odor-specific time cells across days (Pearson correlation, ρ = -0.08; p = 0.96). Cells pooled per animal (n = 5 mice). Shaded grey region denotes the variance across animals.

3.5 DISCUSSION

In summary, here we report the findings that (1) CA3 cells have comparable reliability to CA1 cells, (2) CA3 odor cells do not increase in numbers across days, similar to CA1 odor cells, and (3) CA3 odor-specific time cells do not increase in numbers across days, in contrast to CA1 odor-specific time cells.

We found that CA3 cells have comparable reliability to CA1 cells, but that there may be a less steep drop in reliability between CA3 odor cells and CA3 odor-specific time cells compared to the drop in reliability between CA1 odor cells and CA3 odor-specific time cells. This may indicate a greater stability in the CA3 cell population. To note, we cannot directly compare these findings with those in CA3. Unlike the SI, reliability is not a ratio. Therefore, we cannot discount the differences in methodologies and tools used in that study compared the ones used in this study. Among these differences are that the CA1 study used GCaMP6f, whereas this study utilized GCaMP7f. There is an improvement in the sensitivity and brightness of the newer calcium indicators that could affect reliability calculations. The methodologies differ slightly as well. The CA1 study had a slightly different way to define a cell's firing field and baseline activity. These can also affect the reliability calculations. Given this, what we can conclude is that both CA3 and CA1 have comparable cell reliabilities that drop over time during a DNMS trial. They also share a trend in that the odor cells have higher mean reliabilities compared to mean odor-specific time cell reliability. What is interesting is that while both have this difference between reliabilities in odor and odor-specific time cell mean reliabilities, CA3 seems to have less of

a drop in reliability between odor and odor-specific time cell than CA1 does; In CA3 the difference is around 8%, whereas for CA1 it is around 20%. Again, we can't draw hard conclusions due to the differences in methodologies and tools used in the two studies, but this difference between the two cell groups is large enough that it warrants comment. We can compare the differences in reliability between the two cell groups in CA1 and CA3 with less concern, because we are now comparing trends rather than specific numbers. If this trend is true, then CA3 cells could be more reliable than CA1 cells because their reliability is more stable and consistent across time.

We found that CA3 odor cells do not increase in numbers across days. Similarly, CA1 odor cell population did not increase across days (Taxidis et al., 2020).

We found that CA3 odor-specific time cells do not increase in numbers across days and are not affected by learning. In contrast, the CA1 odor-specific time cell population was found to increase over days (Taxidis et al., 2020). CA1 odor-specific time cells were found to increase in number as the DNMS performance accuracy increased (Taxidis et al., 2020). Bayesian time decoding error in CA1 significantly decreased across days, inversely correlating with odor-specific time cell population increase (Taxisdis et al., 2020). Odor decoding in CA1 did not change across day (Taxidis et al., 2020). Taxidis et al. postulated that CA1 odor-specific time cells increased because more information was being stored within the time cells. This contrasts with our findings that CA3 odor-specific time cells do not increase in numbers across days. We believe this is the case because the implicit

timing structure of the DNMS task was learned early in the training, mostly likely during the lick shaping step. The odor-specific time cells that hold this information were mostly set before the non-match-to-sample shaping. The temporal structure of the DNMS task is unchanged throughout training. We expect memory consolidation of timing during further steps, but we do not expect the odor-specific time cells to encode additional temporal information. In addition, the mice are not required to learn any new explicit timing rules during the non-match-to-sample shaping. We postulate that the increase in CA1 odor-specific time cell numbers is due to the population encoding temporal signals for anticipation and day-to-day novelty in the environment. CA1 has been found to be more attuned to environmental novelty than CA3 (Leutgeb et al, 2004; Larkin et al., 2014). The anticipation signal could be present in CA1 too. The time decoding error decreases close to end of the trial, as also seen in CA3. This attention to those temporal signals could allow for better time decoding across days. The role of CA3 may be to hold the stable code that give the mouse information on the implicit timing structure of the DNMS task. This information does not change across days, as the delay is fixed. Since the temporal information does not change, it is not surprising that the number of odor-specific time cells does not change across days. In this way, CA3 is more stable than CA1, since it holds this stable temporal code. In summary, we believe the CA3 odor-specific time cells hold stable code regarding the fixed implicit timing of the DNMS task. When this information is passed onto CA1, information on novelty and other information on the day-to-day changes in the environment is added, leading to an increase in odor-specific time cells.

These results taken together point towards CA3 having more stability than CA1; CA3 has more stable reliability across time and a more stable odor-specific time cell population. These findings are in line with the literature in the field. CA3 has been found to have more stable trial-to-trial and day-to-day dynamics compared to CA1 when processing spatial memory (Dong et al., 2021). Our results are novel because they explore the role CA3 in nonspatial memory.

3.6 METHODS

Quantification and Statistical Analysis

Analysis of Calcium Imaging Data

Calculating reliability:

Reliability was calculated through custom scripts written in MATLAB (Mathworks, Natick, MA, USA). Reliability was calculated by first averaging estimated activity across all trials in the preferred odor for a cell within a day. We then located the time point of the maximum averaged trial activity. We defined the bounds of the cell firing field as two frames to either side of this time point. Each frame is 1/31 of a second; the firing field is therefore 5/31 seconds, or approximately 0.16 seconds. After defining the cell firing field, we looked at the cell activity in each trial in the preferred odor. A baseline was created based on the mean activity during the one second before presentation of odor 1. A threshold of two standard deviations above this baseline was set. Signal that falls below this threshold are set to 0. We counted all the trials in which there was activity above this threshold within the cell firing field. We calculated cell reliability by dividing the number of trials with activity above threshold in the cell firing field by the total number of trials.

$$\text{Reliability} = \frac{T_a}{T_t}$$

T_a = Number of trials with activity above the threshold in the cell firing field

T_t = Number of total trials

Calculating percent of cells across days:

We calculated the percent of cells across days through custom scripts written in MATLAB (Mathworks, Natick, MA, USA). We found the percent of odor or odor-specific time cells out of all detected cells. The percentage was calculated for each animal on each day of the DNMS task. We graphed this percentage across all days of experimentation.

3.7 SUPPLEMENTARY FIGURES

Supplementary Figure 3.1.

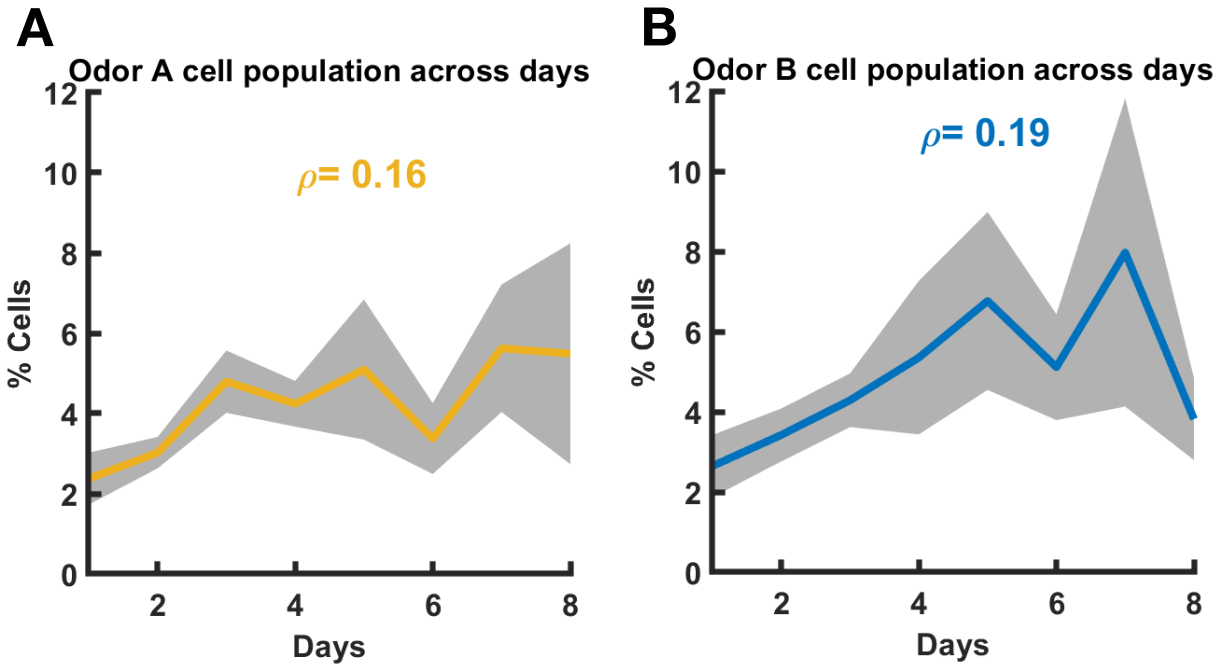

Supplementary Figure 3.1. CA3 odor A and odor B cells do not increase in numbers across days. (A) Mean percent of odor A cells across days (Pearson correlation, ρ = 0.16; p = 0.31) Cells pooled per animal (n = 5 mice). Shaded grey region denotes the variance across animals. (B) Mean percent of odor B cells across days (Pearson correlation, ρ = 0.19; p = 0.24). Cells pooled per animal (n = 5 mice). Shaded grey region denotes the variance across animals.

Supplementary Figure 3.2.

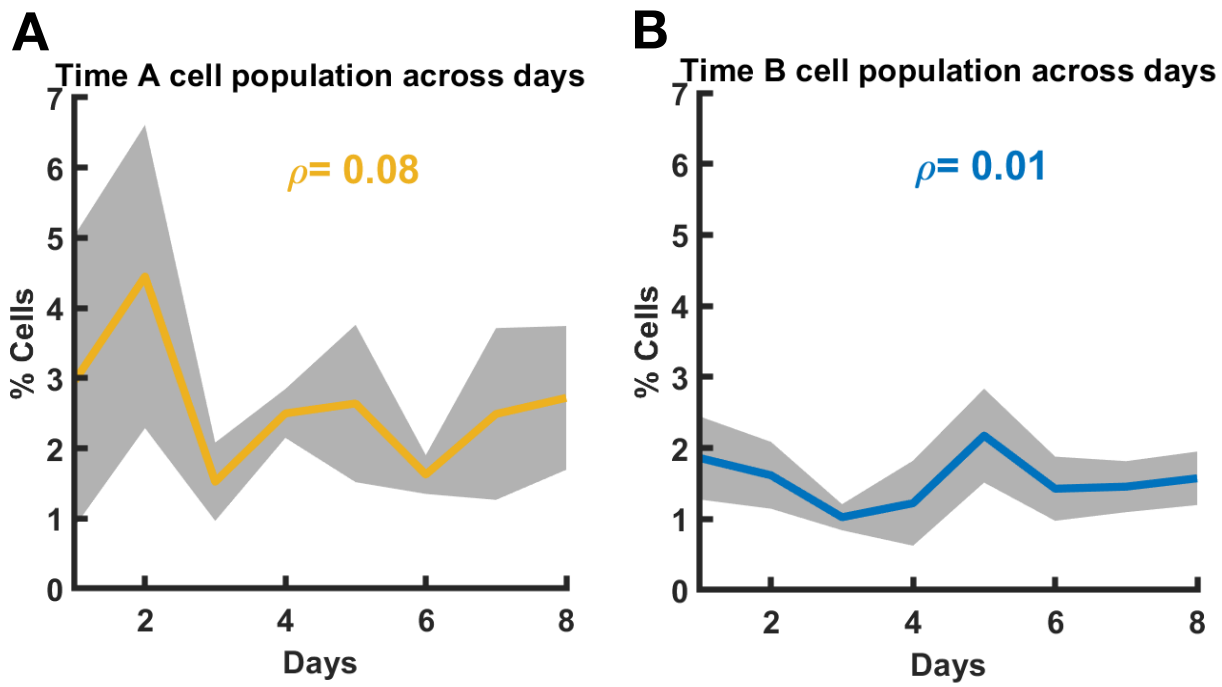

Supplmentary Figure 3.2. CA3 odor-specific time A and odor-specific time B cells do not increase in numbers across days. (A) Mean percent of odor-specific time A cells across days (Pearson correlation, ρ = 0. 08; p = 0.61). Cells pooled per animal (n = 5 mice). Shaded grey region denotes the variance across animals. (B) Mean percent of odor-specific time B cells across days (Pearson correlation, ρ = 0.01; p = 0.94). Cells pooled per animal (n = 5 mice). Shaded grey region denotes the variance across animals.

3.8 REFERENCES

Dong, C., Madar, A.D. & Sheffield, M.E.J. Distinct place cell dynamics in CA1 and CA3 encode experience in new environments. Nat Commun 12, 2977 (2021). https://doi.org/10.1038/s41467-021-23260-3

Larkin MC, Lykken C, Tye LD, Wickelgren JG, Frank LM. Hippocampal output area CA1 broadcasts a generalized novelty signal during an object-place recognition task. Hippocampus. 2014 Jul;24(7):773-83. doi: 10.1002/hipo.22268. Epub 2014 Mar 21. PMID: 24596296; PMCID: PMC4065199.

Leutgeb, S., Leutgeb, J. K., Treves, A., Moser, M.-B., & Moser, E. I. (2004). Distinct ensemble codes in hippocampal areas CA3 and CA1. Science, 305(5688), 1295–1298.

Rolls ET. A quantitative theory of the functions of the hippocampal CA3 network in memory. Front Cell Neurosci. 2013 Jun 25;7:98. doi: 10.3389/fncel.2013.00098. PMID: 23805074; PMCID: PMC3691555.

Taxidis J, Pnevmatikakis EA, Dorian CC, Mylavarapu AL, Arora JS, Samadian KD, Hoffberg EA, Golshani P. Differential Emergence and Stability of Sensory and Temporal Representations in Context-Specific Hippocampal Sequences. Neuron. 2020 Dec 9;108(5):984-998.e9. doi: 10.1016/j.neuron.2020.08.028. Epub 2020 Sep 18. PMID: 32949502; PMCID: PMC7736335.

Chapter 4

Discussion

4.1 SUMMARY OF RESULTS

An open question within neuroscience is: how does the brain process time? In this study, we have tried to narrow down where and how temporal representations are encoded and processed. We hypothesized that sensory and temporal information is integrated in CA3, where a stable code is created and then passed onto CA1.

We began by establishing that CA3 processes sensory and temporal information. We showed that CA3 encodes sensory and temporal information, and that sensory and temporal information can be decoded from CA3 cells.

We characterized how sensory and temporal information is processed in CA3. We found that during a working memory task, CA3 cells fired in a sequential manner. There were cells that were active during the stimuli presentation and then another population of cells that were sequentially active in the delay that followed. Hippocampal sequential activity that tiles a delay is thought to be how the brain carries information in the gaps between stimuli and organizes sequences of events (MacDonald et al., 2011). These “time cells” encode sequential moments in the delay and carry stimuli-specific information (MacDonald et al., 2011; Taxidis et al., 2020). We were able to identify both stimuli-specific cells and stimuli-specific time cells in CA3 during a working memory task. Thus, CA3 uses sequential activity to encode sensory and temporal information.

We further elucidated the properties of the CA3 cells that participated in sequential firing. CA3 sequence cells were found to have low odor selectivity; CA3 odor and odor-specific time cells had low odor selectivity. CA3 therefore has a large population of non-selective sequence cells that hold information on different stimuli. There is a smaller sub-population of sequence cells that are highly selective for odor. These cells have strong odor information and likely hold the odor identity information that is passed onto CA1.

We found that CA3 cells have properties that demonstrate stability. CA3 cells have comparable cell reliability with CA1 cells, and they appear to have a less of a decrease in cell reliability across trial. CA3 odor and odor-specific time cells also do not increase in numbers across days. This contrasts with CA1 odor-specific time cells, which increase in numbers across days and with learning. These measures of stability point at CA3 as a region that can hold a stable code.

How does CA3 and CA1 differ and what roles does each region play in working memory?
CA3 is important for one-trial association and rapid recall (Remaud et al., 2014). CA3 has a unique architecture of recurrent connections that make it a likely region for sequence generation (Treves and Rolls, 1992). CA3 has been postulated to be more stable than CA1. Indeed, it has been found that CA3 cells have more stable properties compared to CA1 cells when processing spatial information (Mizuseki et al., 2012; Dong et al, 2021). CA3 is also important for temporal information. When CA3 is silenced, CA1 temporal coding is disrupted (Middleton and McHuge, 2016). Given this, CA3 is a likely creates a

stable code representing external sensory information and temporal information is integrated and created. This is in line with our results.

CA3 passes a stable sensory and temporal code to CA1. CA1 is important to representing both time (Pastalkova et al., 2008; MacDonald et al., 2011; Kraus et al., 2013) and sequences of ordered stimuli (Manns et al., 2007; Farovik et al., 2010). Crucially, it has also been found that CA1 is critical for distinguishing similar episodic contexts (Kesner and Rolls, 2014). These findings were replicated in human studies (Dimsdale-Zucker et al., 2018). CA1 mainly has feed-forward connections.CA1 receives inputs from other subregions within the hippocampus and other cortical areas. It acts as the main output of the hippocampus. Given these properties, we believe CA1 takes the stable sensory and temporal code from CA3 and incorporates day-to-day and trial-to-trial differences. This is why the CA1 odor-specific time cells were found to be more unstable (Taxidis et al., 2020). CA1 acts as a novelty detector. It can receive other salient information from its inputs, which include the entorhinal cortex, perirhinal cortex, and amygdala, and integrate this with the stable code that is provided by CA3.

4.2 A MODEL FOR CA3

How is time represented in the brain? If time cells encode temporal information, how do their firing patterns represent the temporal context of a memory? There have been three models proposed: (1) Temporal context model, (2) Chaining model, (3) Combined model.

The (1) temporal context model suggests that temporal context signals are sent to the hippocampus from cortical areas. The hippocampus then parses this temporal information into discrete units, which are the time cells (Howard et al., 2014). The time cells organize the information into sequential events through their firing patterns. Each time cell holds unique information that corresponds what information was being processed in the cortex at that moment in time. This model takes into account that many different brain regions have been shown to be involved processing temporal information (Bunhusi and Meck, 2005; Mauk and Buonomano, 2004). This model is unlikely because firing sequences are found to exist in the hippocampus prior to learning (Gragoi and Tonegawa, 2014), meaning they exist in the hippocampus before cortical processing of information. The (2) chaining model suggests that the sequential activity of time cells reflect a chain of firing activity that is generated locally (Mehta et al., 2000). Time cells in this model arise from repeat experiences that increase the strength of sequential connections between cells. This model is less likely. When the timing of a task is extended, instead of adding time cells onto the end of the firing chain, the time cells "re-time," creating a completely new temporal representation of the context (Kraus et al., 2013). The (3) combined model suggests that the hippocampus generates an internal sequential firing chain to represent

the temporal organization of events (Eichenbaum, 2014). The firing chain may be generated at each step and strengthened if the temporal context is salient. This firing chain can be modified by cortical inputs to account for evolving temporal information. The combined model is the most likely model given our current understanding of temporal representations. Time is both an internal and external stimulus. It would make sense that there is both an internally generated sequence and a way for external information to modify this internal code. Where this internally sequence is generated is yet to be elucidated.

This combined model provides a good general framework to think about how the hippocampus encodes time. Expanding on this framework, we believe that while each subregion of the hippocampus receives inputs from the cortex, these inputs are not equal in strength and number. We believe that this is where CA1 and CA3 differ. CA3 receives inputs from the DG and EC. It is most known for its recurrent connections (Witter, 2007). CA1 receives inputs from CA3, CA3, DG, EC, and the thalamus. These inputs each carry unique information that is integrated into memory at CA1. Silencing each input effects different aspects of memory (Nakashiba et al, 2008; Bruin et al., 2008; Suh et al., 2011; Xu and Sudhof, 2013; Hitti and Siegelbaum, 2014). Through its many inputs, CA1 is positioned to receive evolving information and modify the firing chain with the relevant information. We postulate CA3 generates a stable internal code that is not as easily modified by external inputs. Not only does CA3 have less inputs than CA1, CA3 also uniquely has the recurrent connects that allow for sequence generation. There must be a hippocampal subregion that produces a stable firing chain that later can be modified. As

mentioned before, hippocampal firing sequences are found prior to cortical information modification (Gragoi and Tonegawa, 2014). The region that produces this firing sequence would benefit from less cortical inputs. CA3 is one such region.

How does CA3 generate a stable firing sequence? The two main excitatory inputs to CA3 pyramidal neurons are from the DG and recurrent CA3 connections. CA3 receives inputs from the DG through the mossy fibers. A single mossy fiber can make upwards of 37 synaptic connections with the dendrites of a single CA3 pyramidal neuron. Each CA3 pyramidal neuron can receive as many as 72 convergent inputs from DG granule cells (Amaral and Lavenex, 2006). This is in contrast to recurrent CA3 connections. Recurrent connections make several thousand contacts with many more CA3 cells. These connections make up the largest number of synapses on the CA3 pyramidal cell dendrites. This diluted connectivity allows for a higher memory capacity (Rolls, 2013). It allows for the storage of many unique memories and for each memory to be recalled from any one part of itself. Mossy fibers synapse at CA3 apical dendrites near the soma. Recurrent synapses synapse at the distal dendrites. Because of this, a single DG cell can induce CA3 pyramidal firing (Henze et al., 2002), whereas multiple spikes are needed from the recurrent connections (Miles and Wong, 1987) in order to induce CA3 cell firing. While the DG input through the mossy fibers is strong, DG cell firing is sparse (Jung and McNaughton, 1993; Leutgeb et al., 2007).

CA3 performs pattern completion. DG performs pattern separation. The sparse DG firing and small number of mossy fiber connections allows for random cells in CA3 to be activated through DG inputs (Rolls, 2013). This creates different, unique representations to be created in CA3 through DG activation. This allows for many, different representations to be created in CA3 and for the representations to be non-overlapping and non-interfering. These representations then be associated through the abundant recurrent connections, such that any one part of the representation can rapidly recall the whole representation (Rolls, 2013). This is pattern completion. Crucial to this is that CA3 has (1) many recurrent connections, (2) a sparse distributed representation that is enhanced by these recurrent connections. Learning through the recurrent connections can help strengthen or weaken these representations.

Our findings report that CA3 has a small, sparse population of cells that hold information about the sensory and temporal context during a working memory task. This population is largely made of up of non-selective or low selective cells. These cells are active during two distinctive sensory stimuli (two different odors) and over time. There is a small sub-population of cells that are highly selective and hold strong sensory stimuli specific information. This is in line with the previously discussed model of a sparsely active CA3. We propose that smaller, highly selective population correspond to the cells that are activated by the DG inputs. These cells hold the core elements of the representation being passed to CA3. The larger population of low and non-selective cells are quickly associated with the smaller, highly selective population through the CA3 recurrent connections. This

population also allows for the representation to be recalled from any feature of the stimuli. Low selectivity cells can simultaneously hold different aspects of a stimuli. As such, they can be activated by more than a singular stimulus. This allows for efficient recall. We believe that through learning, the selectivity in the small, selective population is increased. Indeed, we found that odor decoding improves after learning, yet the number of odor and odor-specific time cells did not increase. This increase in selectively comes from learning that occurs in the recurrent connections. We postulate it is the smaller, more selective population of CA3 cells that send a stable code to CA1.

4.3. FUTURE DIRECTIONS

CA3 stability across days

It would be interesting to further investigate the stability of CA3. Do the odor and odor-specific time cells keep their identities across days? Or do odor cells re-map into odor-specific time cells and vice versa? We hypothesize that the small, highly selective population of odor and odor-specific time cells do not re-map across days. The larger population of non and low selective cells may re-map to better capture the pieces of information that best help to recall the core, stable memory.

We have already built decoders for time and odor for each experimental day. It would be interesting to test the decoders built on one day with the data from a different day. If decoders from different days can accurately decode odor or time, this would be another indicator of CA3 stability. We would predict that the different day decoders would at least be able to decode odor across days. Decoding time would be less likely, though possible. While CA3 does process temporal information, the DNMS task, as aforementioned, only uses implicit timing, not explicit timing. As such, the temporal context of this task is less salient. Though time can be decoded each day, there may be differences between the encoded temporal context across days. The rule of the DNMS tasks requires a stable, consistent memory of odor, not necessarily time.

Inhibition of CA3

Though CA3 encodes odor and time and may do so in stable manner, it is still not known if information regarding either is processed separately or integrated at CA3. Specifically, it is not known if odor cells firing in CA3 directly drive the sequential firing of odor-specific time cells in CA3 through CA3 recurrent connectivity. An alternate hypothesis could be that CA3 neurons receive inputs from neurons in other brain regions that are already firing sequentially. Furthermore, it is not known whether this activity is required for behavioral performance. It would be interesting to test if time and odor are integrated in CA3 by modulating odor cells and observing if there is an effect on the odor-specific time cells. If there an effect, then odor cell firing will causally drive odor-specific time cell firing, as change in one should cause change in the other. Inhibiting CA3 odor cells evaluates the necessity of CA3 odor cells for accurate behavioral performance and activation of odor-specific sequences. Activating CA3 odor cells tests sufficiency of these cells for accurate behavioral performance and the activation of odor-specific sequences. There is a distinction between inhibition and activation experiments: the former tests necessity, the latter sufficiency. CA3 may be sufficient, but not necessary for processing temporal information. There might be alternative pathways for integrating sensory and temporal information, but activation of CA3 cells might be enough to elicit integration.

We predict that inhibiting CA3 odor cells in well-trained mice during the DNMS task would cause performance accuracy to decrease. Lesioning CA3 has been shown to disrupt performance in a sequential nonspatial memory task (Farovik et al., 2009). Thus, inhibiting

the CA3 odor cells should disrupt performance in the DNMS task. Though, we predict that silencing CA3 odor-specific time cells in well-trained mice during the DNMS task would not have a strong behavioral effect. The salient information that is necessary to accurately complete the DNMS task is mainly odor identity information. Mice must be able to hold the identity of odor 1 and compare it to odor 2. Since timing is not necessary to complete the task, silencing odor-specific time cells may not have a strong behavioral effect. There should still be an effect on the temporal code in CA1. Indeed, silencing CA3 has been shown to disrupt temporal coding in CA1 during linear track recordings (Middleton and McHugh, 2016). It would be interesting to see if we could replicate this in our non-spatial task. Our assay also requires learning and working memory, which could help tease apart the role CA3 has in learning temporal context. Inhibiting CA3 and understanding its effects on CA1 would help us understand how information flows from CA3 to CA1.

Where one might see a behavioral effect is in silencing CA3 odor-specific time cells during learning of the DNMS task. Specifically, silencing CA3 odor-specific time cells during the lick shaping step of learning. In this step, mice are learning the temporal structure of the DNMS task. We would predict that mice with inhibited CA3 odor-specific time cells would still be able to learn the structure of the DNMS task due to cues such as odor and auditory, but we predict that these mice would learn at a slower pace than control mice. The inhibited mice would have to rely on these other cues, delaying their learning.

Reward and feedback signal

We restricted our analysis to the time period starting from odor 1 presentation to the end of the five second delay. In looking at our data, CA3 cells appear to have strong activity following the second odor presentation. This activity could represent a reward or feedback signal. This is especially interesting for CA3 cells because this signal could originate from recurrent connections. It would be interesting to see if the low selectivity or high selectivity cells display more of this activity. The activity after may be recurrent connections strengthening and reinforcing the activity of high selectivity cells or priming new low selectivity cells to be created.

We could also image the recurrent connections simultaneously with the CA3 soma to see if the recurrent connections are a source for this activity following the second odor presentation. We could achieve this by imaging the CA3 soma and the CA3 distal dendrites, where CA3 recurrent connections synapse.

CA3 subarea variability

One of the challenges of this study was that we were unable to precisely mark which subarea of CA3 we were imaging. It is postulated that the different CA3 subareas could have different functional roles. Proximal and distal CA3 receive mossy fiber projections from different positions along the transverse axis of the DG (Cairborne et al., 1986). Functional differences have been found along the DG transverse axis (Hara et al. 1990; Jaarsma et al., 1992; Scharfman et al., 2002; Choi et al., 2003; Witter, 2007). Studies

have also found that dorsal and ventral CA3 have different roles in fear conditioning (Hunsaker and Kesner, 2008; Besnard and Sahay, 2020).

Given this, in the future we would like to mark the region in which we are imaging. This would help us understand what CA3 subarea we are in and to elucidate possible functional differences for CA3 subregions in nonspatial working memory. We could also image a larger region of CA3 using a large field-of-view two-photon mesoscope. This would help overcome the current anatomical challenges of imaging large populations of cells in CA3 and overcome possible variability in CA3 subareas.

4.4 REFERENCES

Amaral, D. and Lavenex, P. (2006) Hippocampal Neuroanatomy. In: Andersen, P., Morris, R., Amaral, D., Bliss, T. and O'Keefe, J., Eds., The Hippocampus Book, Oxford University Press, Oxford, 37-115.

Besnard A, Miller SM, Sahay A. Distinct Dorsal and Ventral Hippocampal CA3 Outputs Govern Contextual Fear Discrimination. Cell Rep. 2020 Feb 18;30(7):2360-2373.e5. doi: 10.1016/j.celrep.2020.01.055. PMID: 32075769; PMCID: PMC7050277.

Brun VH, Leutgeb S, Wu HQ, Schwarcz R, Witter MP, Moser EI, Moser MB. Impaired spatial representation in CA1 after lesion of direct input from entorhinal cortex. Neuron. 2008;57:290–302.

Buhusi, C., Meck, W. What makes us tick? Functional and neural mechanisms of interval timing. Nat Rev Neurosci 6, 755–765 (2005). https://doi.org/10.1038/nrn1764

Claiborne, Brenda J., David G. Amaral, and W. Maxwell Cowan. "A light and electron microscopic analysis of the mossy fibers of the rat dentate gyrus." Journal of comparative neurology 246.4 (1986): 435-458.

Dimsdale-Zucker, H.R., Ritchey, M., Ekstrom, A.D. et al. CA1 and CA3 differentially support spontaneous retrieval of episodic contexts within human hippocampal subfields. Nat Commun 9, 294 (2018). https://doi.org/10.1038/s41467-017-02752-1

Dong, C., Madar, A.D. & Sheffield, M.E.J. Distinct place cell dynamics in CA1 and CA3 encode experience in new environments. Nat Commun 12, 2977 (2021). https://doi.org/10.1038/s41467-021-23260-3

Eichenbaum H. Time cells in the hippocampus: a new dimension for mapping memories. Nat Rev Neurosci. 2014 Nov;15(11):732-44. doi: 10.1038/nrn3827. Epub 2014 Oct 1. PMID: 25269553; PMCID: PMC4348090.

Farovik A, Dupont LM, Eichenbaum H. Distinct roles for dorsal CA3 and CA1 in memory for sequential nonspatial events. Learn Mem. 2009 Dec 22;17(1):12-17. doi: 10.1101/lm.1616209. PMID: 20028733; PMCID: PMC2807176.

Henze, D. A., Wittner, L., and Buzsáki, G. (2002). Single granule cells reliably discharge targets in the hippocampal CA3 network in vivo. Nat. Neurosci. 5, 790–795.

Hitti FL, Siegelbaum SA. The hippocampal CA2 region is essential for social memory. Nature. 2014;508:88–92.

Howard MW, MacDonald CJ, Tiganj Z, Shankar KH, Du Q, Hasselmo ME, Eichenbaum H. A unified mathematical framework for coding time, space, and sequences in the

hippocampal region. J Neurosci. 2014 Mar 26;34(13):4692-707. doi: 10.1523/JNEUROSCI.5808-12.2014. PMID: 24672015; PMCID: PMC3965792.

Hunsaker MR, Kesner RP. Dissociations across the dorsal-ventral axis of CA3 and CA1 for encoding and retrieval of contextual and auditory-cued fear. Neurobiol Learn Mem. 2008 Jan;89(1):61-9. doi: 10.1016/j.nlm.2007.08.016. Epub 2007 Oct 10. PMID: 17931914; PMCID: PMC2675280.

Jung, M. W., and McNaughton, B. L. (1993). Spatial selectivity of unit activity in the hippocampal granular layer. Hippocampus 3, 165–182. doi: 10.1002/hipo.450030209
Kesner RP, Rolls ET. A computational theory of hippocampal function, and tests of the theory: new developments. Neurosci Biobehav Rev. 2015 Jan;48:92-147. doi: 10.1016/j.neubiorev.2014.11.009. Epub 2014 Nov 20. PMID: 25446947.

Kraus, B. J., Robinson, R. J., White, J. A., Eichenbaum, H. & Hasselmo, M. E. Hippocampal 'time cells': time versus path integration. Neuron 78, 1090–1101 (2013).

Leutgeb, J. K., Leutgeb, S., Moser, M. B., and Moser, E. I. (2007). Pattern separation in the dentate gyrus and CA3 of the hippocampus. Science 315, 961–966. doi: 10.1126/science.1135801

MacDonald, C. J., Lepage, K. Q., Eden, U. T. & Eichenbaum, H. Hippocampal 'time cells' bridge the gap in memory for discontiguous events. Neuron 71, 737–749 (2011).

Mauk MD, Buonomano DV. The neural basis of temporal processing. Annu Rev Neurosci. 2004;27:307-40. doi: 10.1146/annurev.neuro.27.070203.144247. PMID: 15217335.

Middleton SJ, McHugh TJ. Silencing CA3 disrupts temporal coding in the CA1 ensemble. Nat Neurosci. 2016 Jul;19(7):945-51. doi: 10.1038/nn.4311. Epub 2016 May 30. PMID: 27239937.

Miles, R., and Wong, R. K. S. (1987a). Inhibitory control of local excitatory circuits in the guinea-pig hippocampus. J. Physiol. 388, 611–629.

Mizuseki K, Royer S, Diba K, Buzsáki G. Activity dynamics and behavioral correlates of CA3 and CA1 hippocampal pyramidal neurons. Hippocampus. 2012 Aug;22(8):1659-80. doi: 10.1002/hipo.22002. Epub 2012 Feb 27. PMID: 22367959; PMCID: PMC3718552.

Nakashiba T, Young JZ, McHugh TJ, Buhl DL, Tonegawa S. Transgenic inhibition of synaptic transmission reveals role of CA3 output in hippocampal learning. Science. 2008;319:1260–1264.

Pastalkova, E., Itskov, V., Amarasingham, A. & Buzsáki, G. Internally generated cell assembly sequences in the rat hippocampus. Science 321, 1322–1327).

Remaud J, Ceccom J, Carponcy J, Dugué L, Menchon G, Pech S, Halley H, Francés B, Dahan L. Anisomycin injection in area CA3 of the hippocampus impairs both short-term and long-term memories of contextual fear. Learn Mem. 2014 May 15;21(6):311-5. doi: 10.1101/lm.033969.113. PMID: 25171422; PMCID: PMC4024620.

Rolls ET. The mechanisms for pattern completion and pattern separation in the hippocampus. Front Syst Neurosci. 2013 Oct 30;7:74. doi: 10.3389/fnsys.2013.00074. PMID: 24198767; PMCID: PMC3812781.

Suh J, Rivest AJ, Nakashiba T, Tominaga T, Tonegawa S. Entorhinal cortex layer III input to the hippocampus is crucial for temporal association memory. Science. 2011;334:1415–1420.

Treves A, Rolls ET. Computational constraints suggest the need for two distinct input systems to the hippocampal CA3 network. Hippocampus. 1992 Apr;2(2):189-99. doi: 10.1002/hipo.450020209. PMID: 1308182.
Witter MP. Intrinsic and extrinsic wiring of CA3: indications for connectional heterogeneity. Learn Mem. 2007 Nov 14;14(11):705-13. doi: 10.1101/lm.725207. PMID: 18007015.

Xu W, Sudhof TC. A neural circuit for memory specificity and generalization. Science. 2013;339:1290–1295.